High-throughput Synthesis and Characterization of Thin-Film Photocatalysts

A Thesis
Presented to the Faculty of the Graduate School
of Cornell University
In Partial Fulfillment of the Requirement for the Degree of
Master of Science

By
Bowen Dong
August 2013

Abstract

Photocatalytic water splitting is a technology used to produce hydrogen fuel with solar energy on the surface of photocatalyst. To make the process to have a high efficiency, the photocatalyst need to be effective visible spectrum, so the most energetic part of solar can be utilized. Developing a visible light photocatalyst for water splitting is a complicated task. It requires study on materials composition, structure, crystallinity and surface modification of a material. The performance of a photocatalyst is valued by its photocatalytic activity, which is characterized by its cutting off wavelength, magnitude of photocurrent at fixed potential and threshold voltage. Besides, the durability and cost of a photocatalyst is also important for overall consideration. Since only a modest number of materials have been explored as candidate materials for photocatalytic water splitting, and because of the complicated nature of the task, it is a good idea to look broadly at a wide range of materials and material combinations in order to identify promising material systems and reveal trends in composition-activity relations. However, a broad survey of potential photocatalytic systems and study on more complex material combinations mean more samples to be processed and measured, which can be time consuming. To solve the problem, we use "combinatorial materials science," a high-throughput method for processing and characterizing new materials, as an approach for experimental study of candidate photocatalysts.

This thesis reports the use of RF reactive cosputtering as a method for synthesizing composition-spread samples and the development of an automated

system for photoelectrochemical characterization. The experimental work is divided into two main sections: the first describes development of a photoelectrochemical characterization system in which we measure the photocurrent generated by samples that are biased with respect to an aqueous electrolyte. The second describes specific experiments aimed at modifying the band structure of tungsten oxide, in order to make its conduction band edge more negative than the reduction potential of H^+/H_2 (0 V vs. NHE at pH = 0). A number of transition metals were incorporated in binary combinatorial oxide samples with tungsten W-TM-O, where TM represents a transition metal such as Fe, Cu, or Zn. The cyclic voltammogram of the resulting films were measured, along with the photocurrent as a function of voltage. These measurements were conducted on many points on the sample, each representing a different composition. Data were measured in a neutral solution environment under 405 nm near-UV laser radiation. We found that W-rich compositions of W-Zn-O exhibit remarkable photoresponse at zero potential (measured with respect to a standard Ag/AgCl reference electrode).

Biographical sketch

Bowen Dong was born in Beijing, China. He a B. S. degree in Applied Physics from Harbin University of Science and Technology. After a one year internship in the China Film Group Corporation, he started his graduate study in Prof. van Dover's group at Cornell University. Two years of research and study in the photocatalytic group, equipped him with new skills in thin film processing and characterization techniques as well as crucial training in conducting independent research and coping with new tasks. In his tenure as a M.S. student he established and improved the experiment setup, and presented his research in a poster session at a national conference. Pressing the work forward granted him precious lab experiences, and prepared him well for future study and work. Also this two-year study in a new culture enhanced his ability to live, communicate, study and do research in a challenging environment.

Acknowledgements

This work was partially performed in CNF (Cornell Nanoscale Facility), a member of the NNIN (National Nanotechnology Infrastructure network), which is supported by the National Science Foundation (Grant ECS-0335765).

I would like to thank my graduate committee: Prof. Bruce van Dover and Prof. Héctor Abruña. They graciously provided their expertise, equipment, and time to help get this project started and have continued to support it to fruition—this thesis.

I would like to express my gratitude to members of van Dover research group for their support and assistance. Specifically, I want to thank Taro Noai and Huanan Duan, who helped me to get started with vacuum technology and sputtering system, and answers my entry level questions patiently. Also I feel express my great gratitude to my former lab mate, Ian Fuller, who established the original experimental hardware setup for characterization. It is because of his early efforts that this research was able to develop as far as it has.

Finally and most importantly, I want to thank my parents, my aunt Jin Huang, and my uncle Qunsheng Song, whose consistent support both financially and emotionally, love and inspiration make it possible for me to keep on and acquire so much in my life and study.

Bowen Dong

May. 23rd 2013

Contents

1. Introduction

1.1 Background

Ever-growing energy demand, pollution and climate change attributed to the burning of fossil fuels, have made the development of alternative energy an urgent concern. Solar energy is the most promising long-term source of renewable energy, and it has already been applied in a large scale with photovoltaic devices. However, it suffers from energy storage problem. Photovoltaic generation is increasingly important but cannot provide electric energy at night unless a capital-intensive large-scale energy storage scheme is employed. Hydrogen is a clean fuel with high energy density that is also relatively easy to store in large-scale facilities. Highly efficient energy conversion technologies for hydrogen fuels, such as fuel cells and internal combustible engines are already available, though an affordable way of hydrogen has yet to be developed. Currently hydrogen fuel is produced either by steam reforming of natural gas or by electrolysis. Neither of these methods is capable of producing hydrogen at low cost. So a technology combining the advantages of the two would be promising. For this reason photocatalytic water splitting draws a huge interest. By utilizing inexhaustible solar energy to produce hydrogen, the future economy could be powered in a clean and renewable way.

1.2 Photocatalysis

A semiconductor can be a photosensitizerthat absorbs photons and generates electrons and holes, causing the simultaneous oxidation and reduction of reactants.[1] In 1972, Fujishima and Honda discovered the water splitting effect using a rutile-structure TiO_2 electrode connected throughan electrical load to a Pt counte electrode, andirradiated with UV radiation.[1] [2] (Figure 1) In the past four decades, a number of other semiconductor photocatalysts have been identified for water splitting applications.

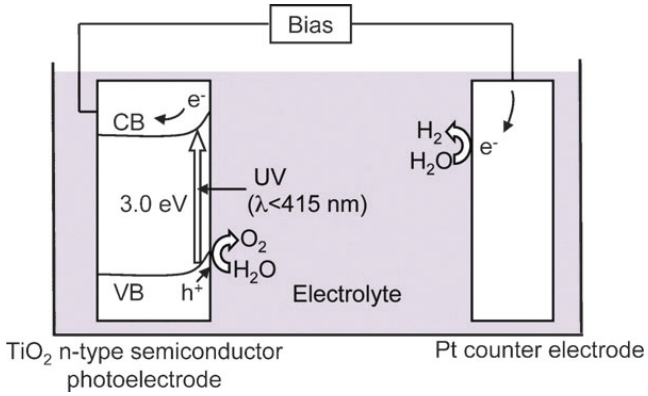

Figure 1 Fujishima experiment set up[3]

To catalyze a redox reaction utilizing the energy of a photon, the conduction band bottom (CB) and valence band top (VB) potentials of a semiconductor photocatalyst must straddle the reduction and oxidation reaction potentials for the reactions involved.[1] The CB must be more negative (higher vs. absolute vacuum energy level) than the reduction half reaction potential, and the VB has to be more positive (lower vs. absolute vacuum energy level) than the oxidation half reaction potential of the redox reaction. (Figure 2)

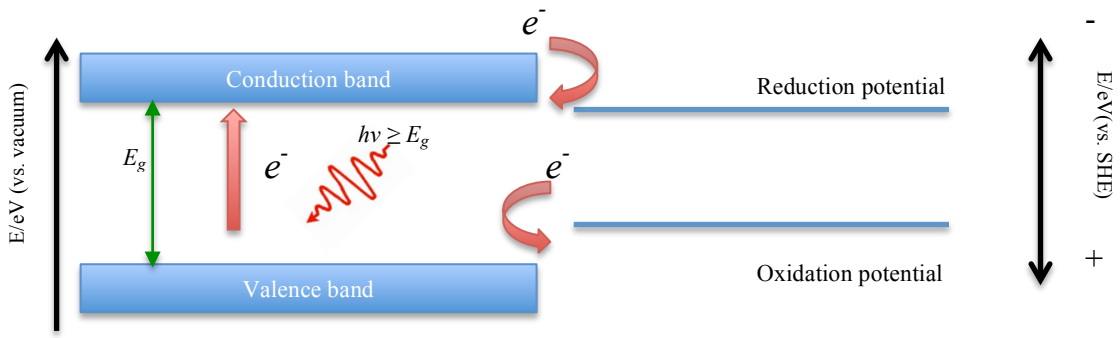

Figure 2 Electronic structures of photocatalyst for a redox reaction and schematics for photocatalysis process.

During photocatalysis by an n-type semiconductor, photons with energy larger than the band gap are absorbed and excite electrons in valence band to the conduction bandy. (Figure 2) The electrons in the CB then move to the surface of counterelectrode to reduce the reactant in a reduction half reaction. Since the VB is more positive than oxidation potential, holes generated from excitation process move to the oxidation level to participate in the oxidation half reaction on the surface of the semiconductor (working electrode).

Photocatalytic water cleavage is an example of photocatalysis as discussed above. In water splitting, the CB and VB of the photocatalyst must straddle the reduction and oxidation potentials, so that photogenerated electrons and holes both participate in the redox reactions. (Figure 3)

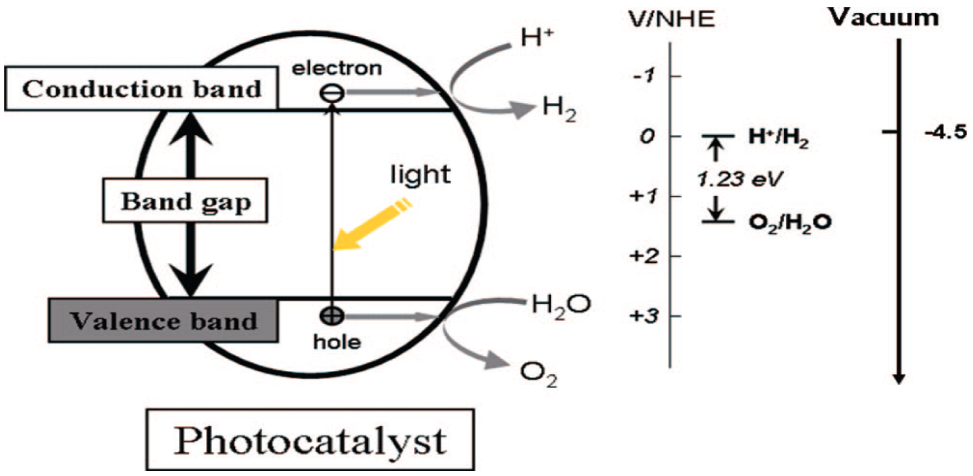

Figure 3 Schematics for photocatalytic water splitting[4]

Thermodynamically, 1.23 eV of photon energy is necessary to drive the process, so only photons with energy larger than band gap energy E_g can contribute to the photocatalysis process. All photons with energy smaller than the band gap would not be absorbed to produce electron-hole pairs, and cannot contribute redox reactions. The band gap of a semiconductor therefore determines the cutoff wavelength for light and therefore the theoretical maximum efficiency for solar energy conversion. ($E = h\frac{c}{\lambda}$) Even materials with adequate values for E_g cannot transfer light-excited charge carriers to participate in the redox reactions if the energy levels of the CB and VB are not located correctly with respect to the absolute oxidation and reduction potentials of water.. The requirement of proper location and appropriate band gap makes it very challenging to identify a semiconductor that might effectively harvest of solar energy this way.

1.3 Visible light photocatalyst

In the past decades, a number of photocatalysts for water splitting have been discovered. They are mostly systems comprising oxides, nitrides, oxy-nitrides and chalcogenides. However no photocatalyst practical enough for industrial use has been developed yet. For one thing, most of those known photocatalysts with a higher efficiency work only in UV spectrum. This means that only photons with very short wavelength can be used. However, only an about 5% of the solar energy is in UV spectrum. (Figure 4) So the major part of solar energy was wasted.

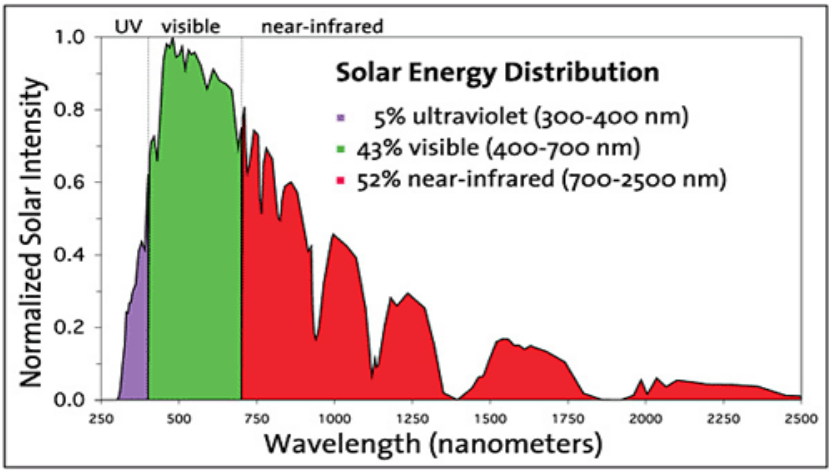

Figure 4 Solar spectra [5]

On the other hand, most of the known narrow band gap photocatalyst such as $(Ga_{0.88}Zn_{0.12})(N_{0.88}O_{0.12})$, cupric oxide[6] and some chalcogenides are not stable enough to survive from the reaction in the solution environment of a photoelelctrochemical cell. Considering these facts, development of durable, high efficiency visible-light-response photocatalyst, would make photocatalytic hydrogen generation one-step closer towards its practical application in mass scale hydrogen fuel production to power the future world.

2. Photocatalyst development, experiment setup and research goals

2.1 Research strategy and band gap engineering

2.1.1 Photocatalytic system selection

Though and materials with proper band structure for visible- response photocatalytic water splitting is yet to be found, a large number of photocatalytic materials have been discovered, and the different functions of elements in photocatalytic system have been revealed. Factors determining the overall performance for a photocatalyst have also been clarified. Band gap engineering theories, high throughput material processing and characterization methods are also making development of such a photocatalyst more efficient than before.

Proper electronic structure is the paramount factor to achieve the goal. But it is hard to find way to make materials with desired band structure easily and economically. However, the known photocatalyst helps to make it easier to begin with, since it is always easier to optimize something than making something from nothing. So in our research, we decide to optimize the performance of existing photocatalyst. For the restriction of our processing method, we limited our searching scope to oxides, nitrides and oxy-nitrides. In order to make it easier to a narrow band gap material working at visible wavelength, oxides with relatively high band gap and poor band location were ruled out from consideration. Since these materials would be used as a work electrode in solution environment in a PEC (photoelectrochemical) system all their lives,

great resistance to electrochemical corrosion would be desired. As W and Ti oxides have been used to protect metals from corrosion, and because they are known as d^0 metal oxide photocatalysts working at UV spectrum, we decided to start with one of them.[4] Because tungsten trioxide has a relatively smaller band gap than titanium dioxide, and because there has been much less research reported on WO_3 than TiO_2, we decided to employ it as our base material. (Figure 5)

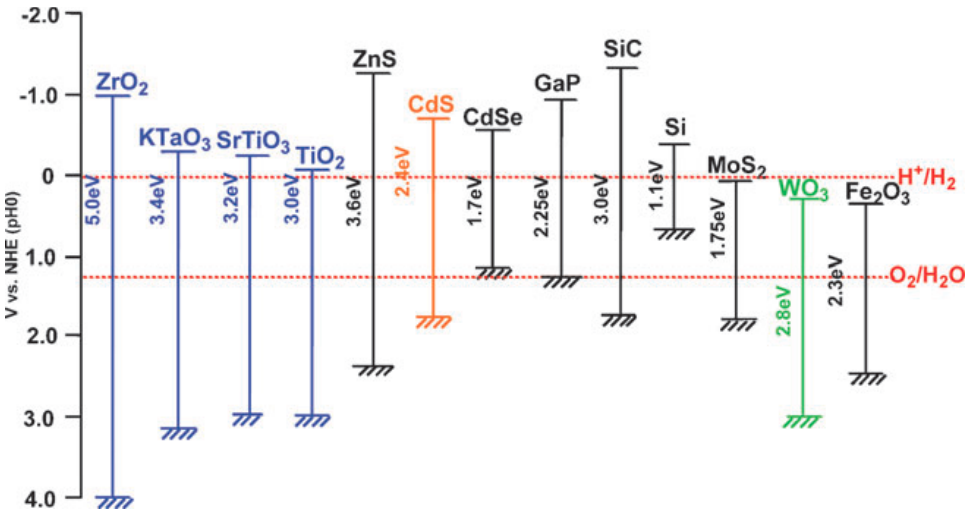

Figure 5 Some band gaps for known photocatalytic systems [7]

However, comparing with TiO_2, WO_3 has an undesirably low conduction band position, even though it has the advantage of a smaller band gap. Hence before attempting to reduce its band gap by bringing up the valence band, we should first focus on moving the position of the conduction band, so its bands can better relate to the redox potential of water. Then we might focus on lowering the 2.4 eV- 2.8 eV band gap [8], so the materials can more efficiently harvest solar energy. The intent of the research in this thesis is to tailor the band structure of W-based oxides.

2.1.2 Band gap engineering

Doping and band coupling are bandgap engineering techniques widely used in development of visible light photocatalysts. [9]

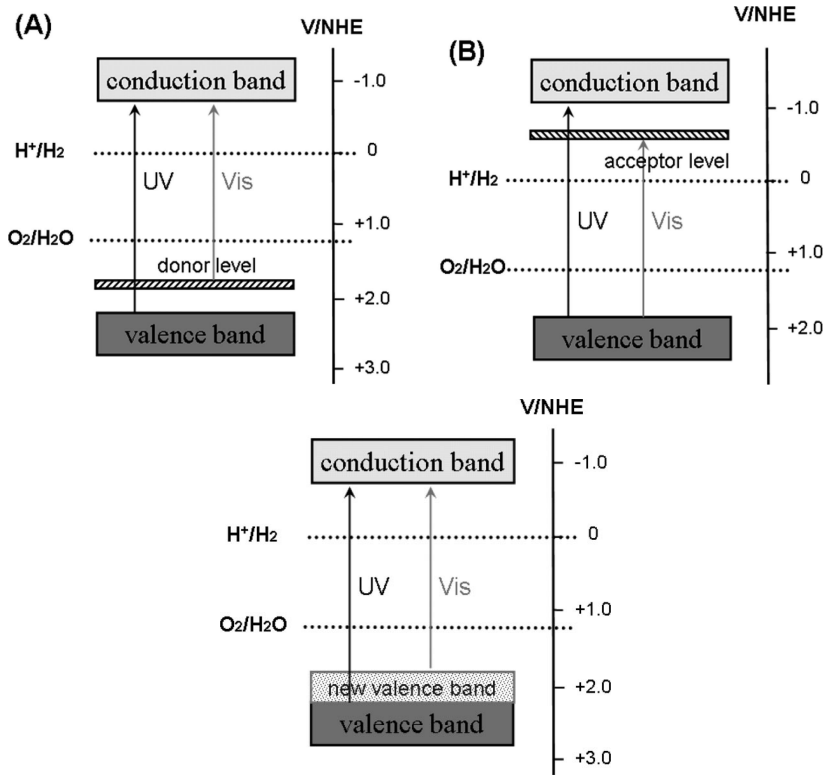

Figure 6 Schematic behavior upon metal doping (top sketches) and nonmetal doping (bottom sketch) [4]

By doping appropriate ions at optimum levels, suitable acceptor or donor levels may be created, reducing the band gap of a UV-sensitive photocatalyst, thereby yielding a photocatalyst with a visible-light response. Doping of metal ions may affect both CB and VB location, while partially substitution nonmetal ions with a lower electronegativity (less positive p orbitals levels) can move the valence band to a more positive location and form a lower band gap as suggested in (Figure 6). Co-doping of metal and nonmetal ions are commonly used in band modification practices. Band coupling is another major way of band gap

engineering. By coupling materials with different band gaps and band locations, smaller band gap and better band location could be realized. (Figure 7)

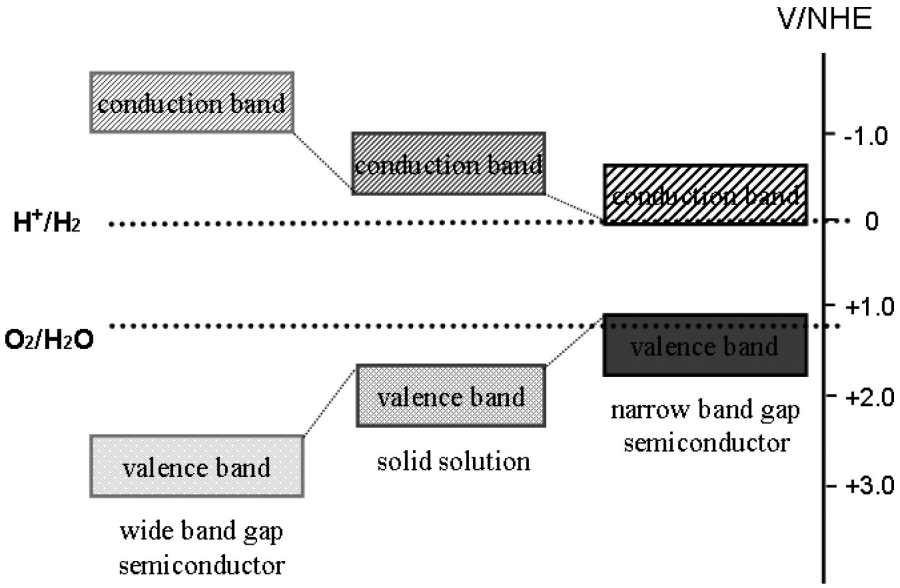

Figure 7 Schematics for solid solution band gap control[4]

2.1.3 Crystallinity and co-catalyst

Crystallinity is of great importance to the development of a photocatalyst. It affects both the bulk and the surface properties for a material. On one hand, the crystal structure of materials determines its final electronic structure, which is the primary consideration for a photocatalyst. On the other hand, point defects, grain boundaries, and surface area of a material determine the performance of charge carrier transport and the chemical reaction. The oxide thin film materials made in our experiments are amorphous, and shows poor performance in photoactivity, and it would be important to make it crystalized. Higher the crystallinity, leads to larger grain size, and fewer grain boundaries and less defects. Since the grain boundaries and defects are the source of bulk recombination, increased crystallinity would effectively minimize charge carrier

recombination within the body, and maximize their probability that electrons and holes migrate to the surface area and participate in redox reactions. (Figure 8 [4][7])

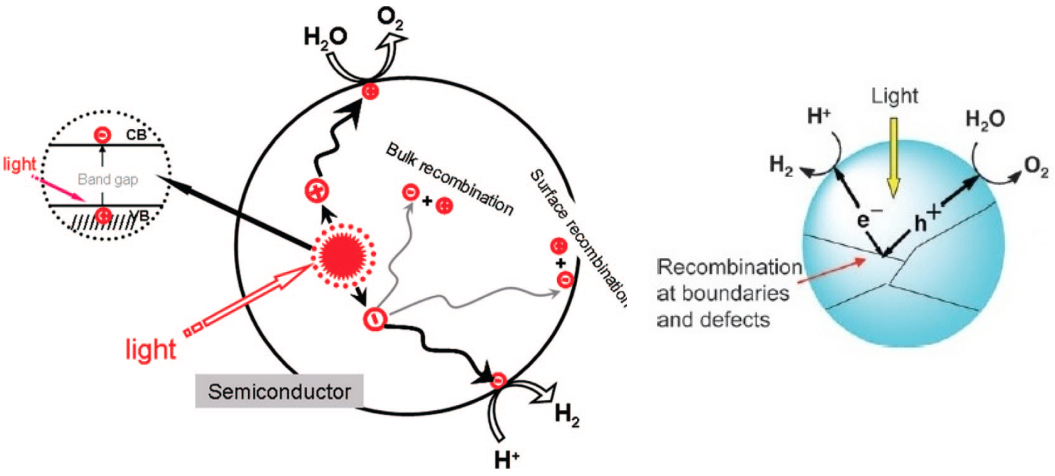

Figure 8 Charge carrier transport [4][7]

Annealing is a straightforward method to induce and increase crystallinity in amorphous and polycrystalline materials. During annealing the crystal structure can change when temperature is increased above a phase transition temperature. A change in crystal structure may alter the band structure, affecting the activity of the material for photocatalysis. The example in Figure 9 shows the behavior of TiO_2 during annealing process. The increasing annealing temperature first changed the material from amorphous form to anatase form, and then from anatase to rutile structure. Following the change in structure, the band gap changed from 3.2 eV of anatase to 3.0 eV of rutile. At the same time, increased crystallinity means larger grains and fewer grain boundaries. It may also lead to changes in surface roughness, increasing or decreasing the effective surface area presented by the thin film to the electrolyte. It is not a priori obvious what

annealing protocol will optimize the photocatalytic response in a given sample; this is best determined experimentally. (Figure 9)

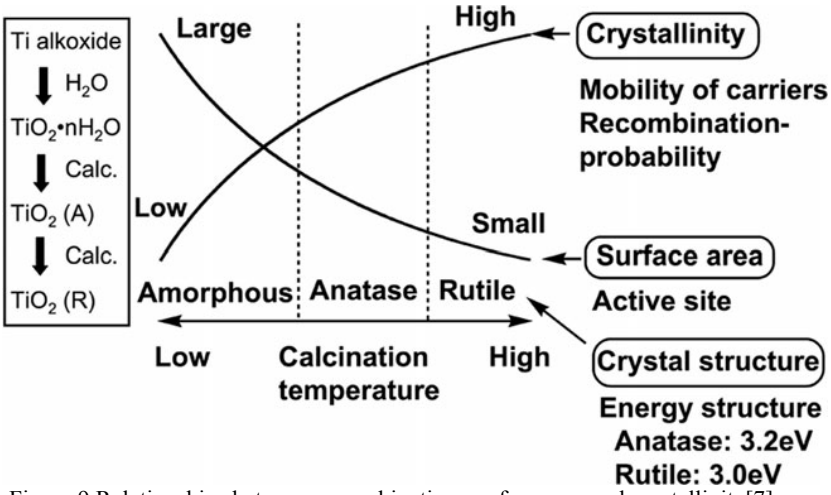

Figure 9 Relationships between recombination, surface area and crystallinity[7]

Loading of a co-catalyst on the surface of photocatalyst is another method for optimizing the photocatalytic response. Co-catalysts can either operate as reaction sites or as reverse reaction inhibitors (oxidation promoter or reduction promoter) for half reactions, and may reduce surface recombination and promote performance of gas generation. Because of their diverse functions on the surface, a combination of two or more co-catalyst may be required for best performance. (Figure 10)

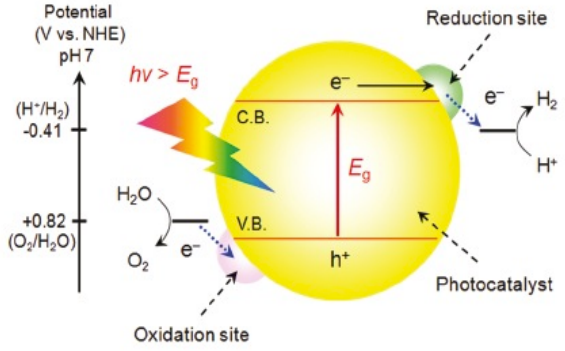

Figure 10 Functions of reaction sites for photocatalysis[10]

Noble metals and some transitional metal oxides have been used as reaction sites for a long time. Because their Fermi level energy is always lower than that of the semiconductor, and as a result of their chemical stability, noble metals can provide energy level for charger carriers to dwell, while not reacting with them. For this reason, photo-generated electrons can be stored in lower energy levels of noble metals, rather than be annihilated with the holes in surface recombination. So photo-excited charge carriers can have a higher probability to participate in the redox reaction on surfaces of electrodes.[4] Pt, Rh, Pd, RuO_2 and NiO_2 have been reported to be superior co-catalysts that provide reaction sites to intensify gas generation on the surface, though they act as reaction sites for both forward water splitting reaction and the reverse reaction. The reverse reaction reduces the efficiency of the process, and must be prevented, so reaction promoters that inhibit the reverse reaction are introduced. A core-shell structure combining the reaction sites and reaction promoters has been developed. (Figure 11). In the recent literature, Cr_2O_3 and Mn_3O_2 were reported to be a good reduction promoter and oxidation promoter respectively, since they can selectively inhibit the oxygen or hydrogen ions from reaching reaction sites. If combined with reverse inhibitive shells, reaction sites would not be affected by reverse reaction and so would provide improved performance.[10] Incorporating this approach in new materials is a long-term goal for the research thrust that governs this thesis.

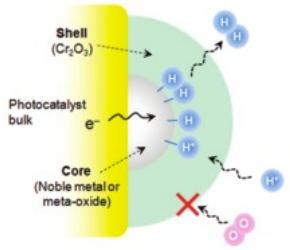

Figure 11 Schematic core shell structure on the surface that might improve the reaction kinetics [10].

2.1.4 Element selection

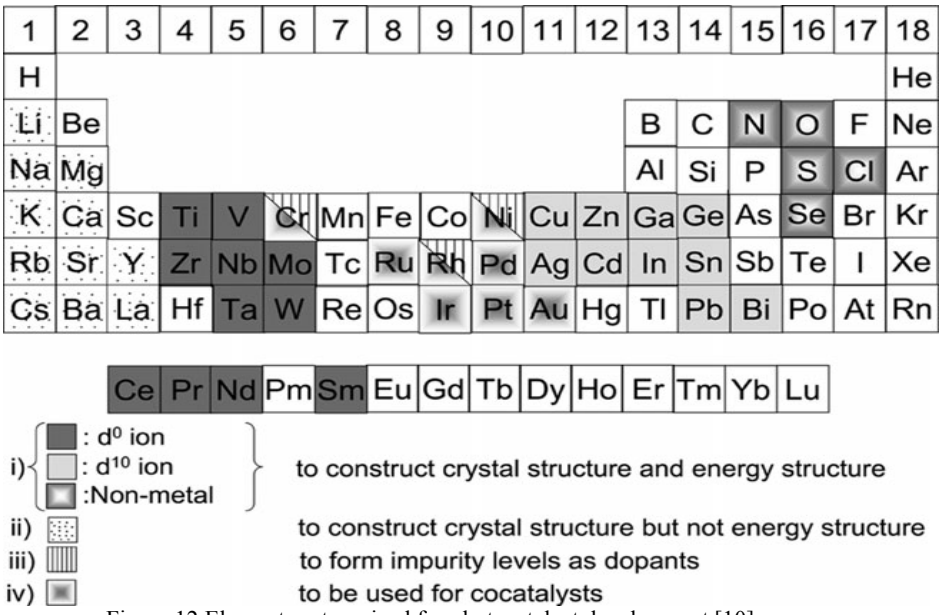

Figure 12 Elements categorized for photocatalyst development [10]

Following the discussion on photocatalytic semiconductor selection involving considerations of bandgap, mechanisms for bandgap engineering, and incorporation of co-catalysts allows us to develop a rational strategy for our research aiming identifying and developing a viable system for photocatalysis using solar radiation. Various elements can play different roles in a photocatalytic materials system, as illustrated in Figure 12.

However, the choices and be further narrowed for our experiments. The alkali metals and alkaline-earth metals are too reactive to be processed in a PVD

system, and are precluded from our 'element pool'. Cd, Se, and S are toxic and can contaminate the vacuum chamber, are also excluded. So a reduced element selection list for our experiment has been established as illustrated in Table 1.

Electronic structure modification metals (Doping or solid solution related metals)	Valence band location modification nonmetals	Co-catalyst providing surface reaction site/ reverse reaction inhibitor
Ti, V, Zr, Nb, Mo, Hf, Ta, Mn, Fe Cu, Zn, Cr, Bi	O, N, Si	Cr, Mo, Co, Ni, Ru, Rh, Pd, Ir, Pt

Table 1 Element selection

2.1.5 Research goals

So far, the basic background, mechanism, and element selection for different purposes in the development of a visible-light-response water splitting photocatalyst has been reviewed. The strategy for our research, which would be concentrating on engineering the band gap and surface modification for tungsten oxide to make it an effective visible light response photocatalyst for solar hydrogen generation, has been confirmed. However, to finish such a task, we would have to overcome at least three obstacles. First the electronic band structure for tungsten oxide, which has a CB more positive than H^+/H_2 potential, has to be modified by incorporating with other elements into WO_3 lattice, so the

band of the resulting solid solution can meet the redox potential requirement of water splitting.[11] (Figure 13)

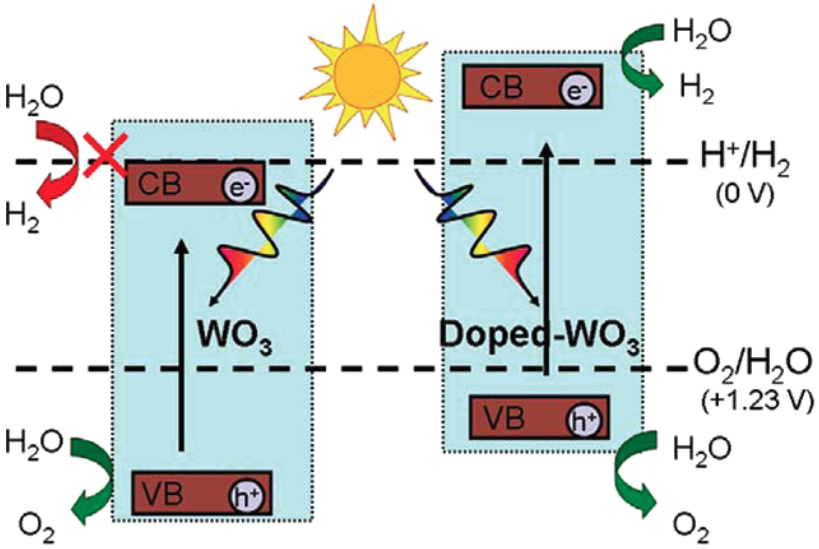

Figure 13 Schematics for proposed band structure modification[11]

With a suitable band location, a clear photocurrent signal should be observed, when a purple laser is irradiated on the sample serving as a working electrode (the material) at zero potential (no bias voltage) in our experiment PEC device. Based on the combination substantiated to have correct band structure, we would change its crystallinity by annealing to find the best annealing temperature for the oxide sample to produce the highest photocurrent in zero voltage. Detailed information about the structure and element ratio for the optimized binary oxide system can be extracted by XRD characterization, while the precise direct band gap can be measured by spectroscopy methods. The second step for the study would be focusing on reducing the band gap of combinatorial oxide. We would try to incorporate p-block nonmetal elements such as N and Si as mentioned before to lift VB for the material without destroying the structure and photo-response property acquired from the previous

step. Step three would be about surface modification, in which we would try to develop and build a core-shell structured co-catalyst to realize gas generation and discuss the overall efficiency of the visible light photocatalyst. The three steps are the primary goals for the whole project. For the even longer run, we will study the effect from thickness for visible-light-response photocatalyst. By studying the diffusion length, light absorption length, and optical coupling, a optimized photocatalyst with even higher efficiency is expected to be developed, which would be very close to a practical one for applications out of the lab.

2.2 Instrumentations and experimental setup

2.2.2 Combinatorial sample processing

As a result of the limitation in theories, and the complicate nature for the problem, a trial and error styled research would have to be conducted. Because multiple elements would be involved in the process of band gap engineering and surface modification, myriad of the ratio configurations for the resulting system need to be investigated. So a daunting number of samples would need to be processed. If we take annealing temperature into the account, then this already daunting number would become several times larger. It could cost researchers all their lives to make and characterize samples in a conventional experiment approach, which produces one sample each time. So it would be inefficient and even impossible to finish our task of developing a highly efficient visible-light-response photocatalyst in a regular way. To cope with this difficulty, a combinatorial synthesis approach for sample processing is employed.

2.2.2.1 Combinatorial synthesis

Combinatorial synthesis has been put into the development of novel materials with desired properties since the mid 90s, and it provides materials scientists the ability of a sample library with a huge number of samples with gradually changed ratio of different compositions in a single experiment. This method has undergone great refinement and has become widely used in the research of high temperature superconducting materials, giant magnetoresistance materials, composites, polymers, catalysts, and biomaterials. Development of specialized vacuum equipment has made it popular for the development of thin-film materials.[12] In our research, a combinatorial reactive sputtering system is used to produce combinatorial oxides, nitrides, or oxy-nitride material libraries on 3-inch wafers.

2.2.2.2 The sputtering system "Fenris"

The RF magnetron reactive co-sputtering system in our group that is configured for 90° off-axis combinatorial thin-film deposition is referred to as "Fenris.". This system was used to synthesize all of the combinatorial materials libraries used in our experiments. (Figure 14) Three Angstrom Onyx-2 magnetron guns incorporating 2-inch targets are mounted horizontally at 90° intervals around a vertical axis at the center of the chamber. Substrates are positioned horizontally at that center, and are therefore perpendicular to the plane of each target ("90° off-axis"). A relatively high gas pressure used in this technique, so the deposition rate falls rapid as a function of distance from each

gun. The sputter guns are energized simultaneously to give codeposition; thus the configuration allows us to deposit ternary or binary combinatorial libraries on silicon wafers. (Figure 15) Ar is used as the dominant gas that provides the high scattering rate required for off-axis deposition, while being nonreactive, and O_2 is added to form oxides during deposition. MKS mass flow controllers are used to precisely control the gas flows. A heater mounted on the sample holder is used to make thin films at temperatures up to 300 °C during deposition.

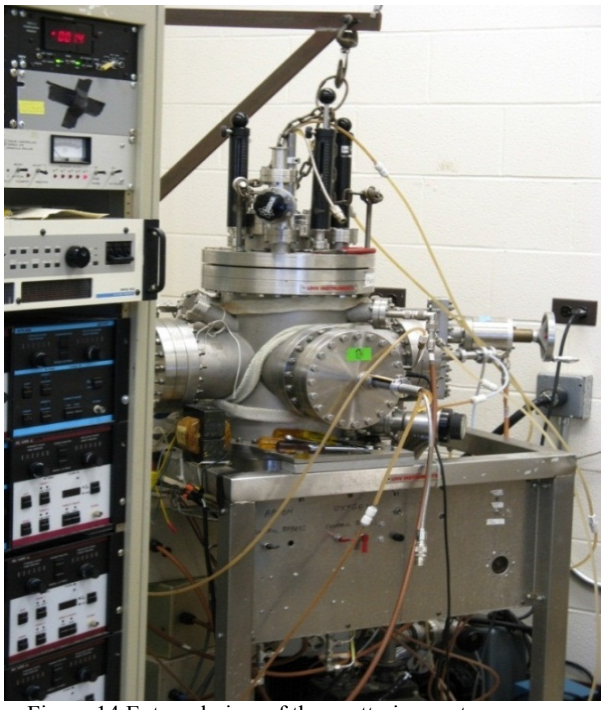

Figure 14 External view of the sputtering system

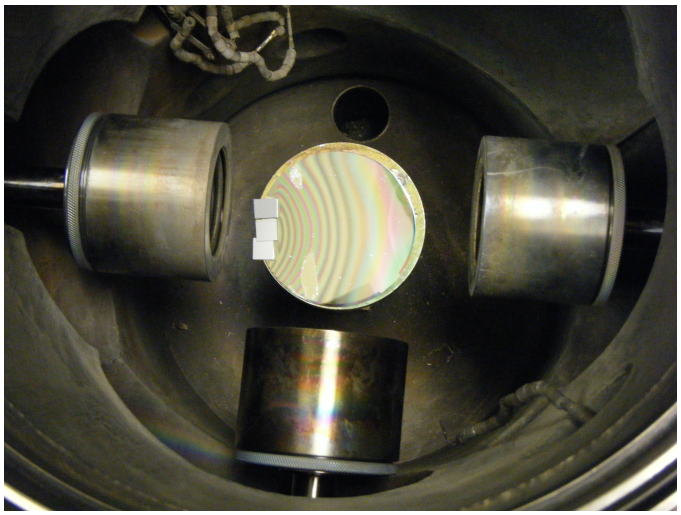

Figure 15 Top view of the three sputter guns inside the chamber, with a 3-inch diameter Si substrate on which a composition-spread film has been deposited.

In the RF reactive magnetron sputtering process, Ar atoms are ionized to be Ar ions. Ions and electrons are accelerated by the RF electric field for each of the half cycle, and they ionize more energetic particles during this process. More and more energetic species are generated until stabilized plasma is formed. The magnetic fields from the magnets below each of the targets in the sputtering guns confine the electrons, accelerating them in the crossed electric and magnetic fields so that they spiral near target surfaces. This maximizes their ionizing collisions with Ar atoms and therefore provides strong bombardment by Ar^+ ions on the targets. Impact of Ar^+ ions on the metal target surface atoms provides enough energy to overcome bonding. The metal atoms are ejected from the surface and impinge and condense on the substrate. The deposited metal atom layers are oxidized by oxygen molecules flowing into the chamber to form oxides on the substrate. If N_2 is introduced as well as O_2, oxynitrides can be synthesized. The use of RF power is important for reactive sputtering, since

insulating oxides inevitably form on the target surface. These oxides impart a large DC impedance (blocking) but represent a negligible capacitive impedance at RF frequencies.

2.2.2.3 Sample processing

Having discussed the theory and described the generic synthetic tool, it is time to describe the core details of this research. To begin with, I will describe the processing of our samples and then discuss the techniques I used to measure the properties that we are looking for.

The process begins with 3-inch p-type silicon wafers. First we anneal them in the air using a Thermolyne 48000 box furnace at 1000 ˚C for 3 hours to grow an 11nm thick SiO_2 layer for insulation. Then the oxidized wafer is coated with a 10 nm Ti adhesion layer and a 25 nm Pt layer by e-beam evaporation in the Cornell Nanofabrication Facility. For the adhesion layer, Ti was chosen rather than the more usual Cr to avoid electrochemical corrosion during the electrochemical measurements. Pt is used as the base electrode since it is unlikely to be oxidized during deposition of the oxide composition-spread film. (Figure 16 and Figure 17)

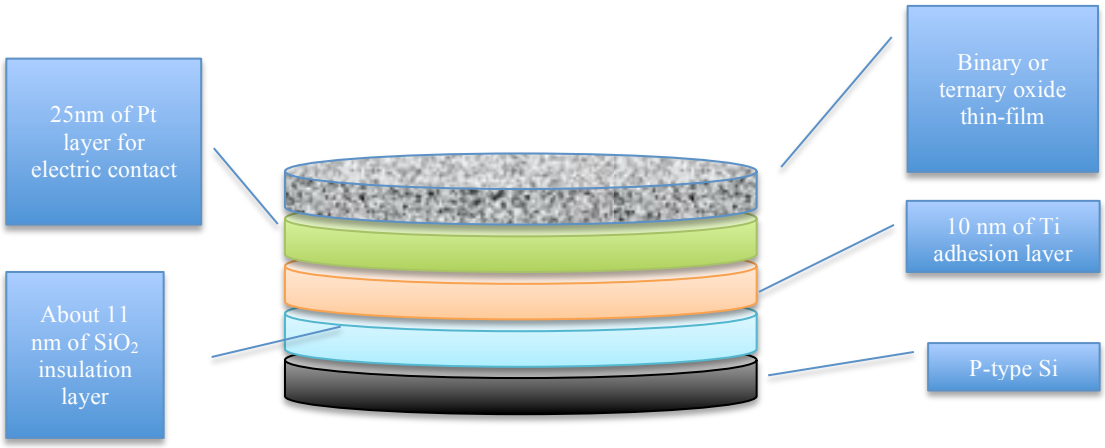

Figure 16 Structure of wafer pre- treated

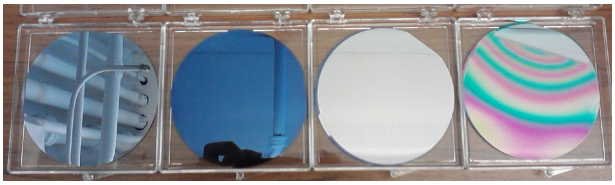

Figure 17 Pictures of wafer after each steps of the processing from the left to the right: P-type wafer, annealed wafer, wafer after Ti and Pt evaporation, Binary combinatorial sputtered sample

After preparing the coated Si wafers, we co-sputter our combinatorial film on the Pt layer. A composition spread is created due to the deposition rate variation with distance from each of the three sputtering guns. (Figure 18) The sputtering rate for an element is highest at points on the wafer closest to the sputter gun, and decreases quickly decreases as the distance from the gun increases. Thus a combinatorial library can be created with a composition distribution as shown schematically in Figure 18. The variation of sputter rate also leads to a change in thickness for different part of the film, even when materials are deposited simultaneously from opposite sides. Visible interference fringes are typically observed on the surface and are due to changes in the optical thickness (physical thickness times the index of refraction). (Figure 19) A small region of the sample is masked during deposition to later provide good contact to

the underlying Pt. As our oxide film is a poor conductor, there would be a large IR drop from the contact to the region of laser illumination unless a good conductor is used underneath. The underlayer must exhibit good corrosion resistance in case there is any pinholes in the oxide film that expose it to the electrolyte. With these two considerations in mind, Pt was chosen as the underlayer to provide a low electrical resistance. Pt does not adhere well to SiO_2 so a thin Ti layer is used as an adhesion layer. (Ni, which is sometimes used as an adhesion layer is not used here, as we found that it exhibits poor electrochemical stability.)

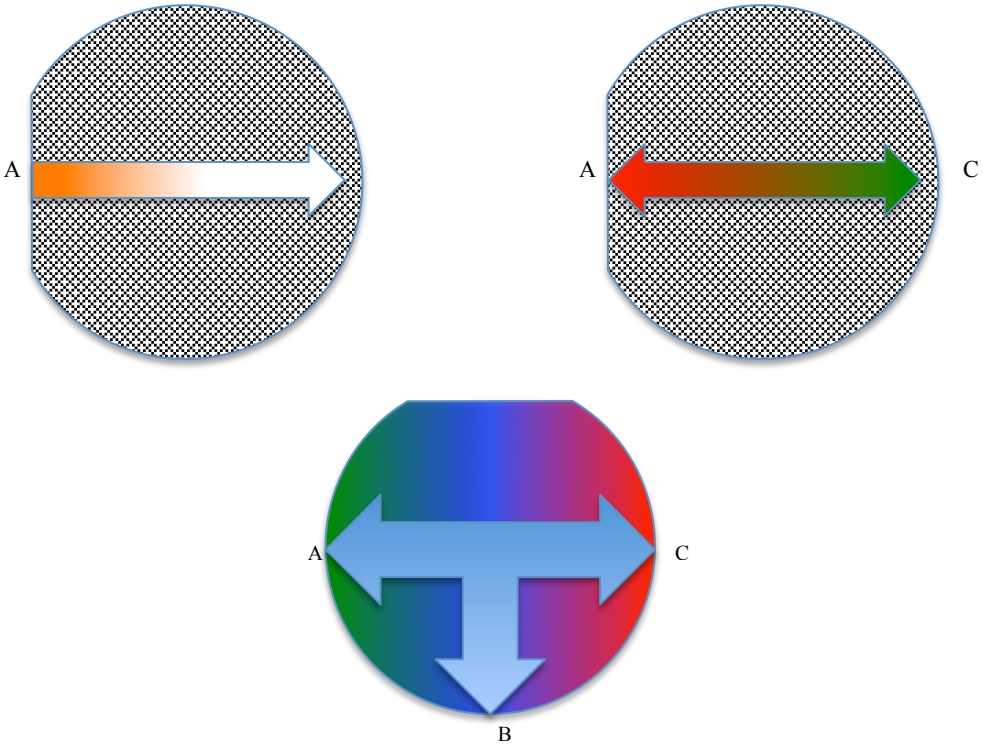

Figure 18 Configurations for single, binary, and ternary material depositionsThe upper left plot shows the materials distribution for a single material deposition; The upper right plot shows the materials distribution for binary oxide codeposition; The bottom plot shows distribution geometry for ternary codeposition.

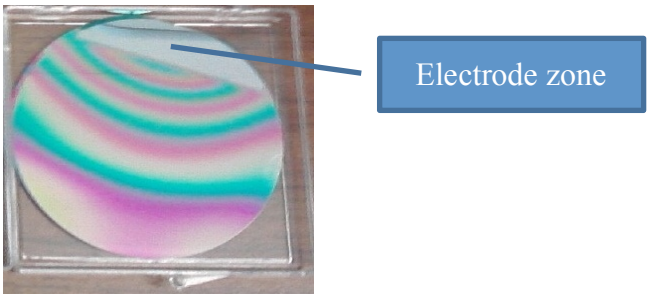

Figure 19 The masked region on the substrate exposes bare Pt so that good contact can be made to the film.

The combinatorial samples typically amorphous as deposited, especially if deposited on room-temperature substrates. Thus they must be postannealed to achieve crystallinity. Considering the symmetry of the oxide composition distribution in single material and binary samples, these can be cleavedinto three equivalent slices that can be annealed at different temperatures. Ternary composition spreads must be annealed as a whole as there is no redundancy in composition. (Figure 20) We annealed samples at temperatures between 500 ˚C and 700 ˚C. Temperatures lower 500 ˚C did not crystallize the films, and temperatures above about 800 ˚C induced delamination and discoloration attributed to reaction with the substrate. The ramp rate for the temperature was set to be 100 ˚C/h, as we found that higher rates often caused delamination.

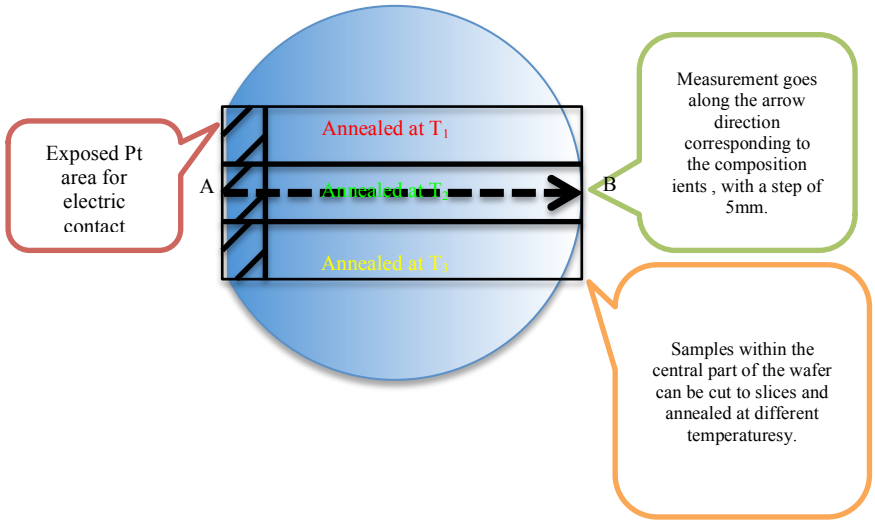

Figure 20 Schematics for the cutting and annealing single material and binary samples

2.2.3 Characterization

2.2.3.1 Instrumentation and experiment setups

Our characterization system is based on a photoelectrochemical cell constructed in our lab. It is composed of both hardware and software systems. The hardware can be further divided into mechanical part and electrochemical part. (Figure 21) The sample is attached to a X-Z stage made up of two ThorLabs 150 mm linear motorized stages. The motion is precisely controlled by a ThorLabs BSC102 stepper motor controller, which provides an ActiveX interface for LabVIEW. By moving the sample with the X-Z stage, the beam from laser pointer will irradiate different positions on our sample, so the photoresponse for different compositions can be measured. Three lasers can be mounted to serve as light sources. The first one is a 1mW, 632.8 nm He-Ne gas laser (Metrologic, Inc.). The other two are laser diodes: a 5 mW, 532 nm core series laser and 25 mW, 405 nm E2 series lasers (Wicked Lasers, Inc.). These provide photons with energy at 1.96 eV 2.33 eV, and 3.07 eV, respectively,

which makes it possible to infer the approximate regions of the visible spectrum in which our photocatalyst is functional.

The sample serves as the working electrode and is immersed in the electrolyte bath together with an Ag/AgCl reference electrode, and Pt counterelectrode. The counterelectrode is a 3-inch oxidized Si wafer with 25 nm of Pt on its surface. In order to determine photoinduced current, a Stanford Research Systems chopper was employed. The chopper is set to running at 40 Hz to provide a clear photocurrent signal for our observation in characterization VI interface. Electrical measurements were done with a PINE AFRDE5 bi-potentiostat. with its output digitized by a National Instruments PCI- 6227 data acquisition card (Figure 22)

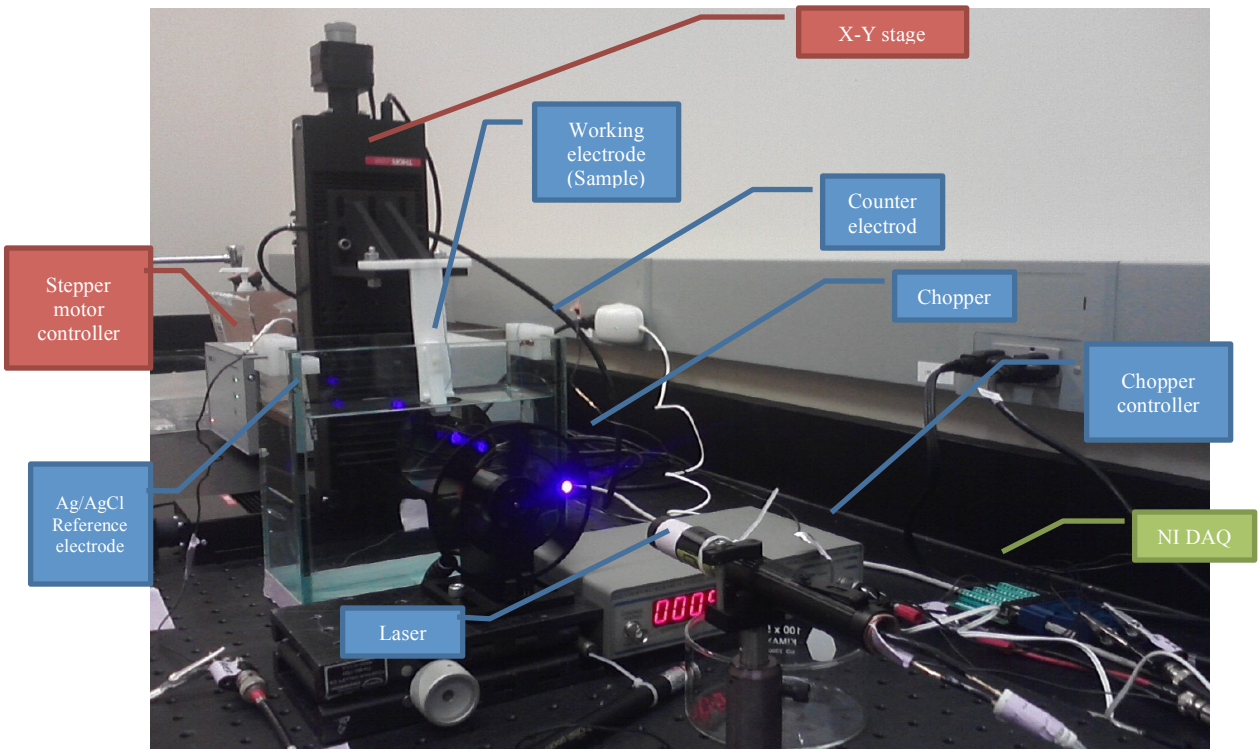

Figure 21 Schematics for the characterization system

Red: Mechanical parts for X-Z position control; Blue: Electrochemical parts, including pen-type laser and large glass container for electrolyte; Green: data acquisition unit (controlled by computer).

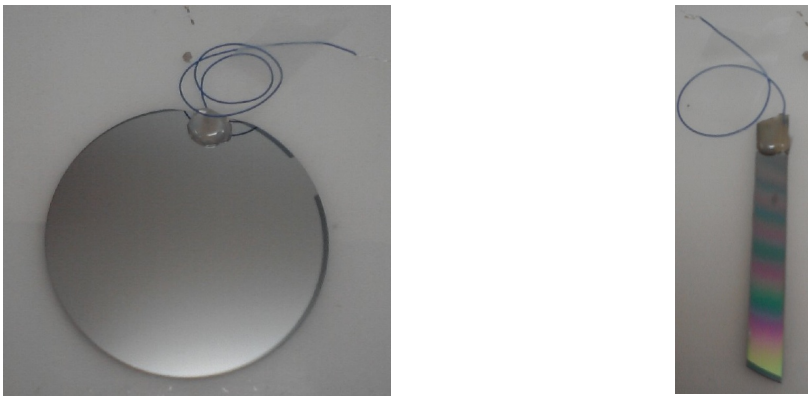

Figure 22 Left: Counter electrode; Right: A typical working electrode (binary oxide composition spread sample)

The potentiostat is used to control the relative electric potential of working electrode to the electrolyte, i.e., the relative band locations of the oxide material towards the redox potential of water can be controlled. (Figure 23)

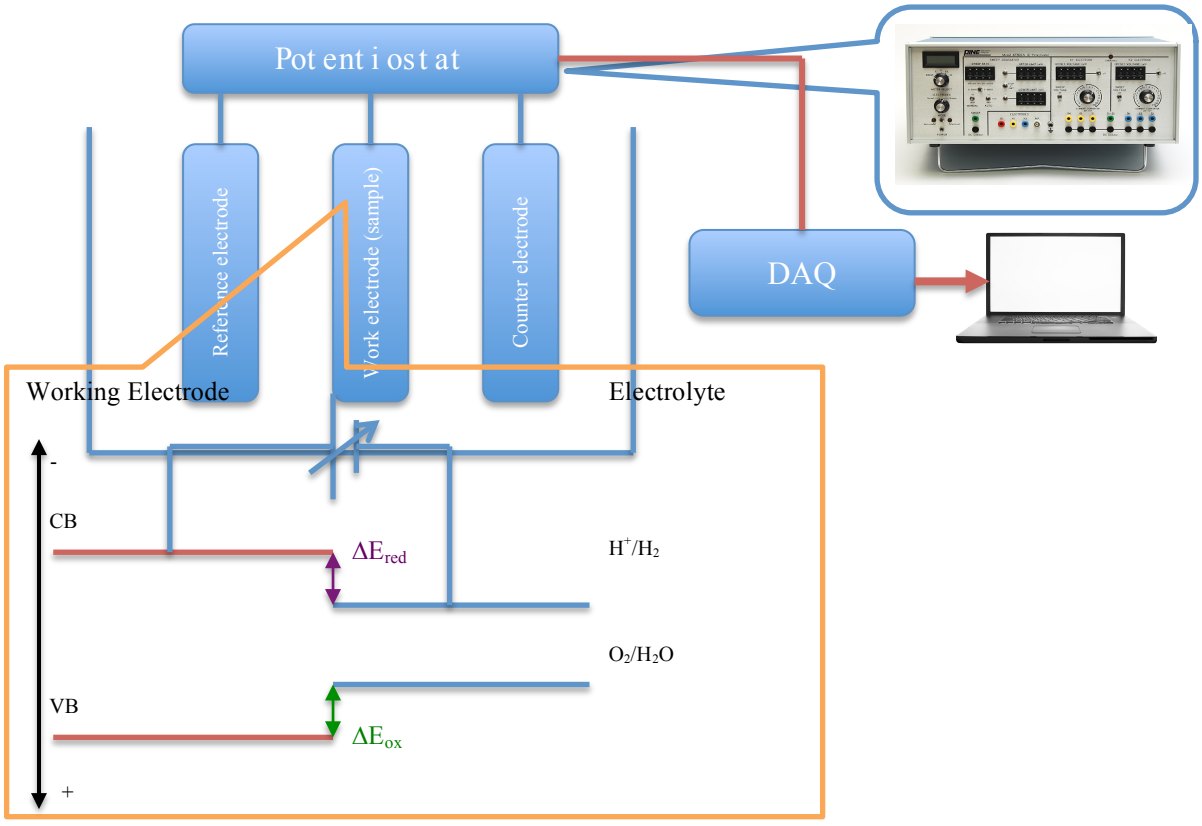

Figure 23 Configuration of the electrochemical system.

The current and electrolyte potential (measured vs. Ag/AgCl reference electrode) are collected using a NI data acquisition card and are presented and analyzed with a LabVIEW program. (Figure 24)

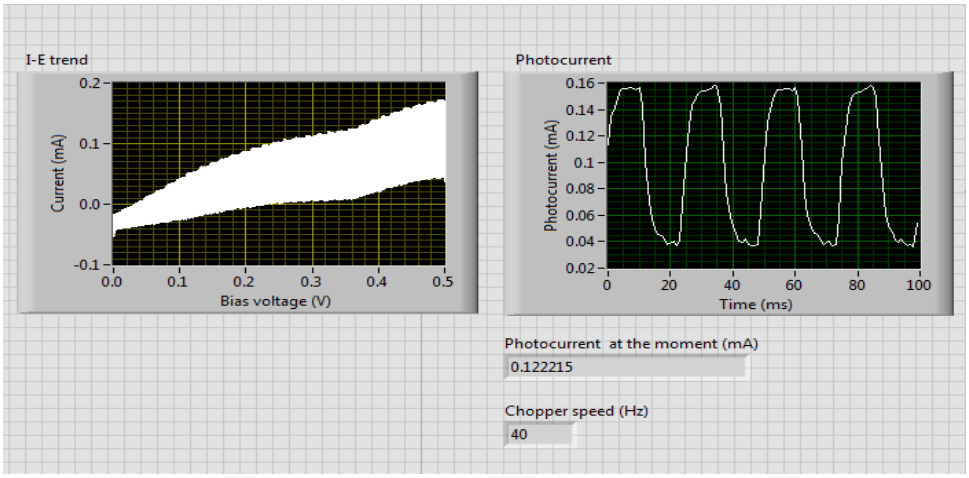

Figure 24 LabVIEW VI interface

The left scope shows the variation of photocurrent vs. potential (vs Ag/AgCl ref electrode). Since the beam illuminating our sample is chopped, both light on and light off signal is presented here. The upper bound of the area is the photocurrent during light on, while the lower bond of the area is the light off dark current. The middle scope shows the light on/ off signal vs. time, showing the photoactivity at the moment.

The display on the left shows the variation of current from working electrode as a function of potential. The display in the center shows a rolling view of the working electrode current in light-on and light-off conditions. Under the center display is a numeric indicator that shows the peak-to-peak voltage difference of the current from working electrode, that is, the photocurrent. The numeric indicator above the color ramp shows the potential of the working electrode relative to the electrolyte.

2.2.3.1 Characterization routine and evaluation

In order to study the band structure, photo-activity and stability of our combinatorial thin film oxide samples, we used the following routines in our

research. First, camera photos were taken of for our thin-film samples, after deposition, annealing, and photocurrent measurement, to enable qualitative observation and documentation for each step. If the film peels after annealing or shows corrosion after photocatalytic characterization, this indicates a poor stability. Photocurrent data was observed by sweeping voltages linearly from 0 V to 0.5 V in the buffered (pH=7) KDP solution. Initial studies use the 405 nm laser since any material with a bandgap up to ~3 eV will absorb photons from this source.

At each location on the sample the photoresponse at zero voltage is recorded first, serving as an indicator of the ability of the oxide semiconductor to absorb photons and create electron-hole pairs. When the potential is increased to positive values an increase in photocurrent is typically observed. This corresponds to O^{2-} oxidation at the working electrode and either H_2 formation or reduction of dissolved O_2 at the Pt counterelectrode. The photocurrents typically increases monotonically so the maximum photocurrent is reached at the terminal value for the ramp, 0.5 V. We therefore record the photocurrent at 0.5 V for each sample point measured. By plotting this current vs. location the sample point showing greatest photoresponse can be immediately identified. By comparing the curves plotted using data collected from samples of the same binary system deposited with the same condition and annealed at different temperatures, the best annealing temperature for a binary system can be located. (Figure 25 and Figure 26)

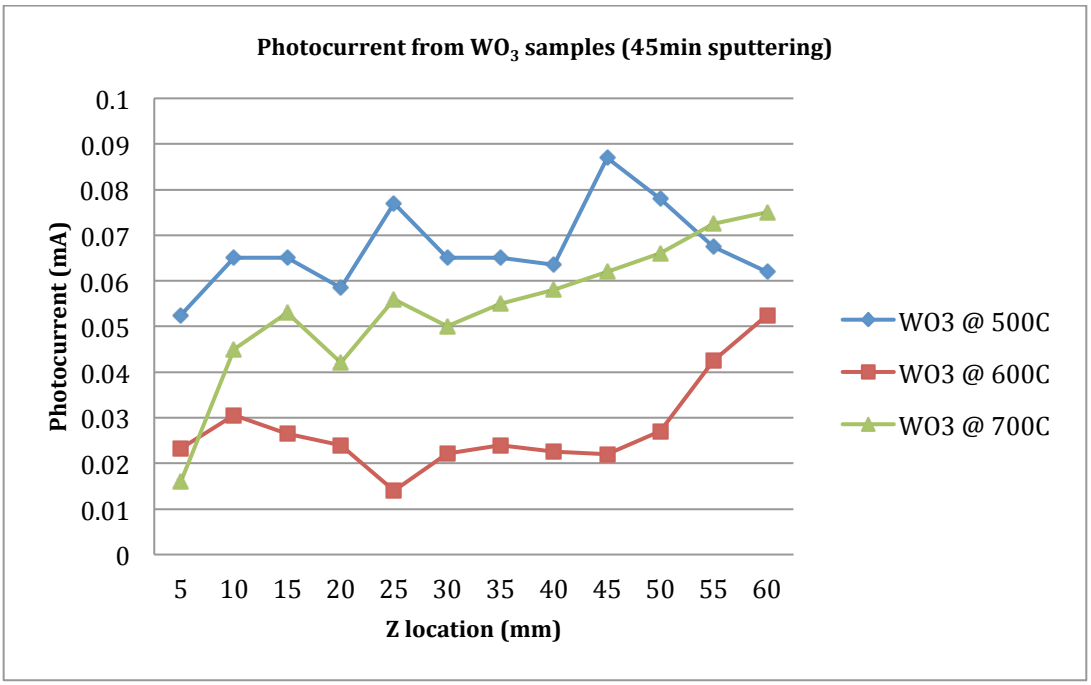

Figure 25 Photocurrent measured at +0.5 V for WO_3 samples annealed at temperatures as indicated. The thickness of the WO_3 varies as a function of position (thicker for higher values of Z).

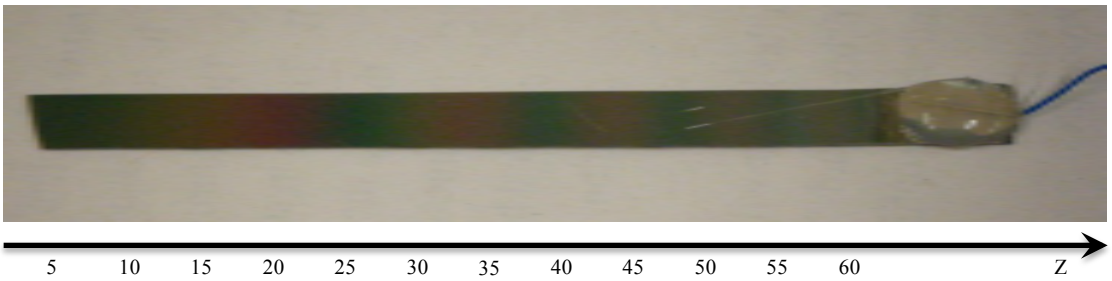

Figure 26 Coordinate system used in our experiment

By ramping the potential of the working electrode to negative values we can look for suppression of the oxygen oxidation and possible hydrogen reduction at the working electrode. (Figure 23) Potentials higher than 0.6 V are typically found to degrade for our WO_3 or WO_3-based thin-film working electrodes, tentatively attributed to the formation of hydrogen tungsten bronzes.[13] In any case attempting to establish a potential higher than 0.7 V can is found to greatly reduce the lifetime of our Pt thin-film counter electrode. Limiting the voltage

scan to the range -0.5 V < E < +0.5 V still allows us to screen for materials that might serve as solar photocatalysts operating without external bias.

3. Results and analysis

3.1 Experiment data and analysis

A variety of transitional metal elements were co-sputtered with WO_3 to determine the effect on electrochemical behavior and photocatalytic activity, with the ultimate goal of identifying a stable material that meets the requirements for spontaneous photocatalytic water splitting. The photoresponse in buffered (pH=7) KDP solution (2500mL solution, made up with 919 mL of 0.1 M NaOH, and 1580 mL of 0.1 M KH_2PO_4) was measured using 405 nm and 532 nm laser radiation. The photocurrents at 0.5 V for each of the sample points on the different composition spreads samples were collected, plotted, and compared.

WO_3

Undoped tungsten oxide films were deposited by sputtering a W metal target at 30 mTorr for 45min with gas flow rates of 10 sccm O_2 and 40 sccm Ar (i.e., 20 vol% O_2). The substrate was then cut into three slices that were annealed at 500 ˚C, 600 ˚C, and 700 ˚C. The photocurrent and threshold voltages for those three samples were measured. This data serves as a control for our studies of binary (two cation) oxide materials based on tungsten oxide as the common cation.

Stability

The stability of tungsten oxide thin film was found to be acceptable, in the sense that no delamination or dissolution was observed during annealing process and photocatalytic characterization. (Figure 27)

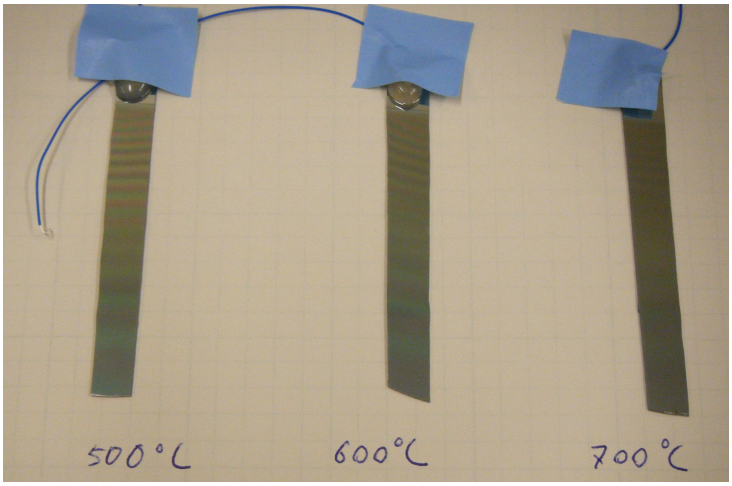

Figure 27 Samples annealed at different temperatures after photocatalysis characterization

Photocatalytic property

Undoped WO_3 showed no photocurrent at zero potential, consistent with reports in the literature. A photocurrent appears when the potential of the work electrode increased above a threshold voltage that depended on the position measured, i.e., the thickness of the WO_3 film, as illustrated in Figure 28. The photocurrent at 0.5 V also depends on WO_3 thickness and is plotted in Figure 28. The overall trend is that the photocurrent increases with increasing WO_3 thickness up to the maximum thickness tested here, ~1.5 (estimated based on optical interference fringes). The total flux of photons absorbed by a semiconductor follows Beer's Law, so this result implies that the absorption coefficient for WO_3 is significantly greater than 1.5□m. For holes to diffuse to the surface of the semiconductor and participate in oxygen oxidation means that

the recombination distance must also be greater than the thickness. Variations in crystalline quality (impurities, grain boundaries, and point defects) may account for local deviation from the overall trend. The threshold voltage shows a distinct maximum as a function of position along the thickness spread. We would expect the threshold voltage to be independent of thickness for a given material with fixed band alignment. However, the threshold voltage is not a reliable measure of thermodynamic potentials; we attribute the variation to possible systematic variation in the film surface morphology as a function of growth rate/thickness. Further study is indicated, including, for example, X-ray diffraction studies to determine if there is a systematic trend in crystallographic texture.

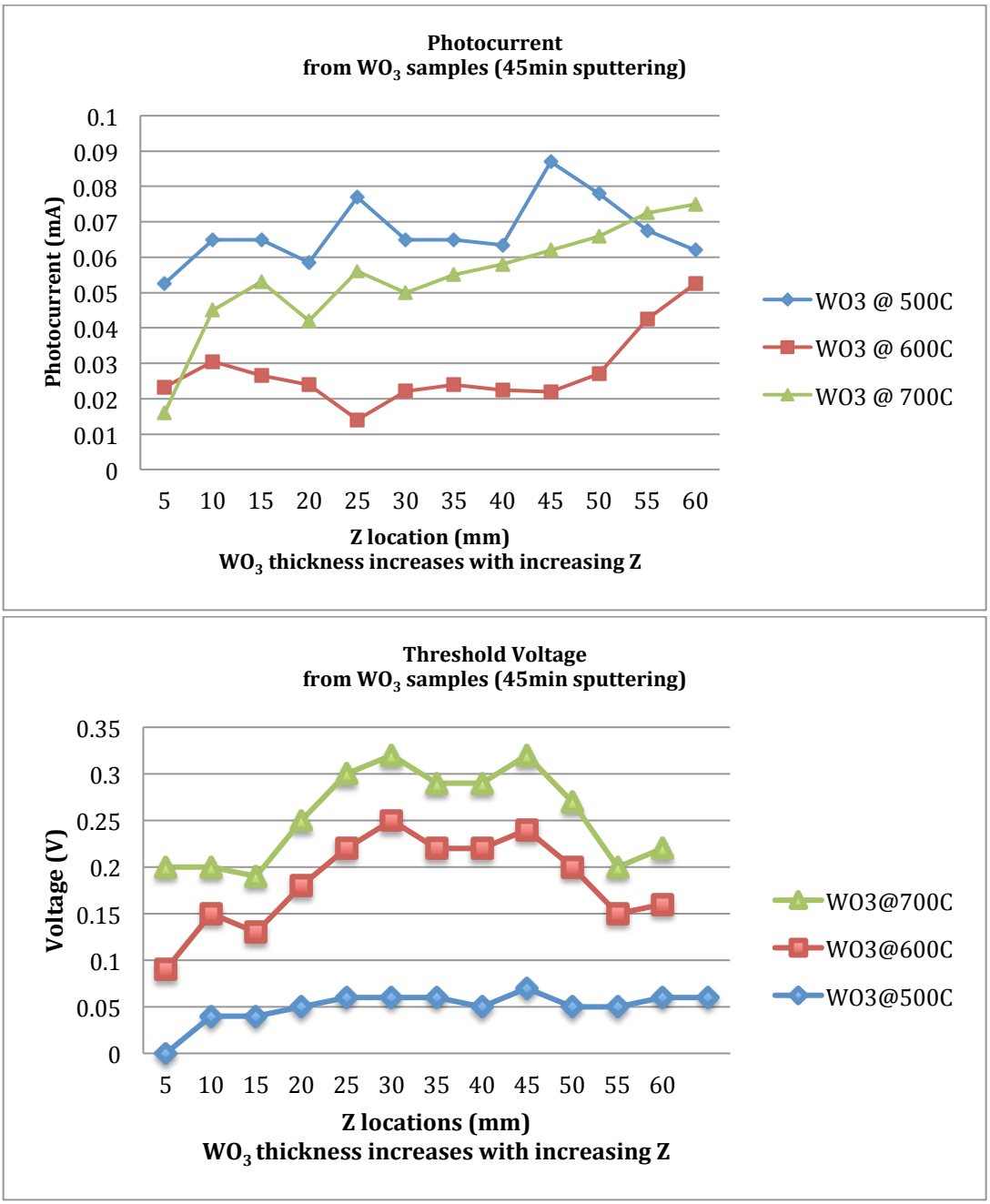

Figure 28 Photocurrents and threshold voltages for tungsten oxide annealed at different temperatures

W-Hf-O

First principle calculations by Fenggong, et al., [11], [14] suggest that Hf-doped WO_3 might serve as a photocatalyst with ideal band locations for water splitting. If experimentally demonstrated this could be a breakthrough material

for solar hydrogen production. The proposed band structure would lead to spontaneous reaction under solar illumination. A relatively small potential might be needed to make it an effective working electrode in a photoelectrochemical cell system for gas production. Motivated by this calculation, we prepared binary composition-spread thin films of W-Hf-O. The films were postannealed in air at temperatures ranging from 500 °C to 700 °C to examine the effect of crystallinity on function.

Stability

W-Hf-O thin films were cosputtered using 100 W of RF power applied to each of the guns. As with undoped WO_3 films, the deposition system was run at 30 mTorr using a 20 vol% O_2 environment, and the deposition proceeded for 40 minutes. The sample was cleaved into three slices for annealing. However, stability in this binary system was poor. Even with a low ramp rate (100 ˚C/h), all three samples suffered degradation. (Figure 29)

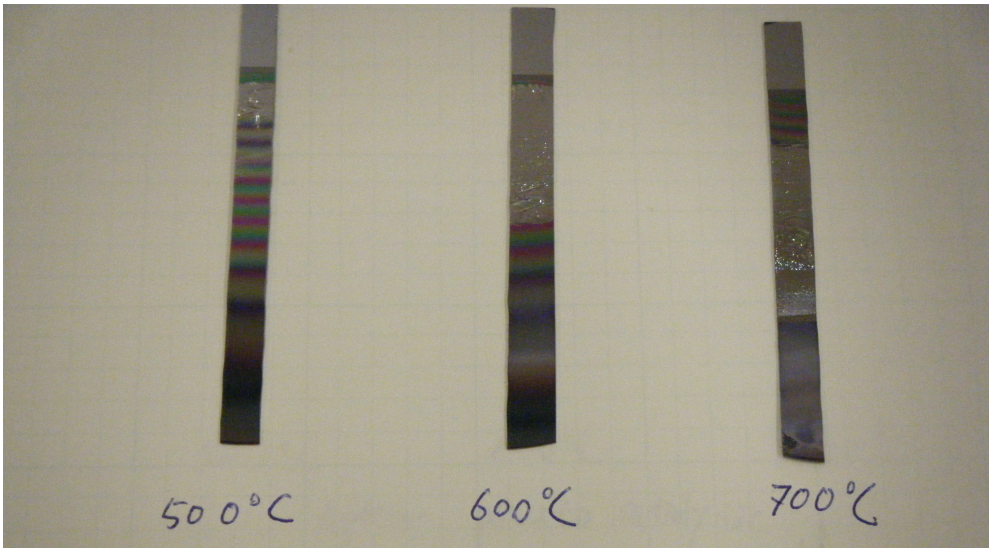

Figure 29 W-Hf-O samples after annealing

Although several attempts were made, only the samples annealed at 500 ˚C were sufficiently intact as to allow photoelectrochemical measurements to be conducted.

Photocatalytic properties

No spontaneous photocurrent signals were observed at zero potential when illuminated with 405 nm laser radiation, and no improvement in the magnitude of the photocurrent at +0.5 V was seen compared to the undoped WO_3. The photocurrent at +0.5 V is about ten times smaller than that of the undoped WO_3 film annealed at 500 ˚C, and the onset potential increased as well. No photocurrent at all was observed for 532 nm (green) laser illumination. The poor stability and photocatalytic performance led us to look for alternative dopant materials. (Figure 30)

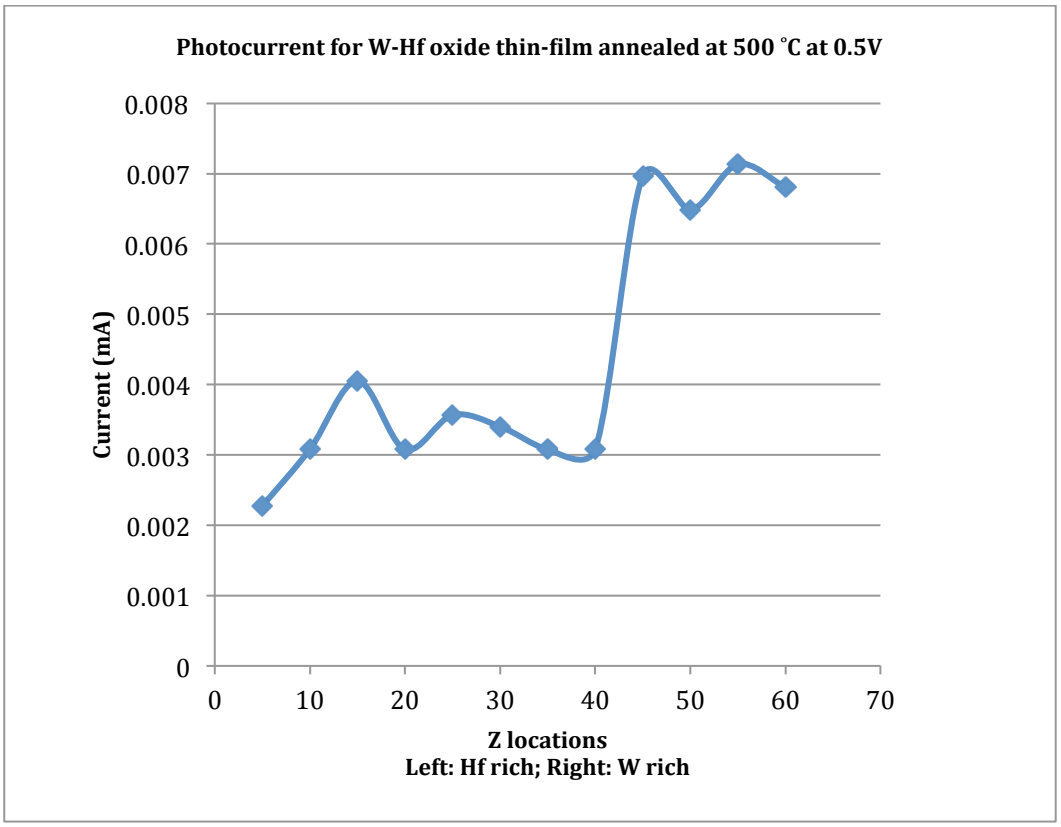

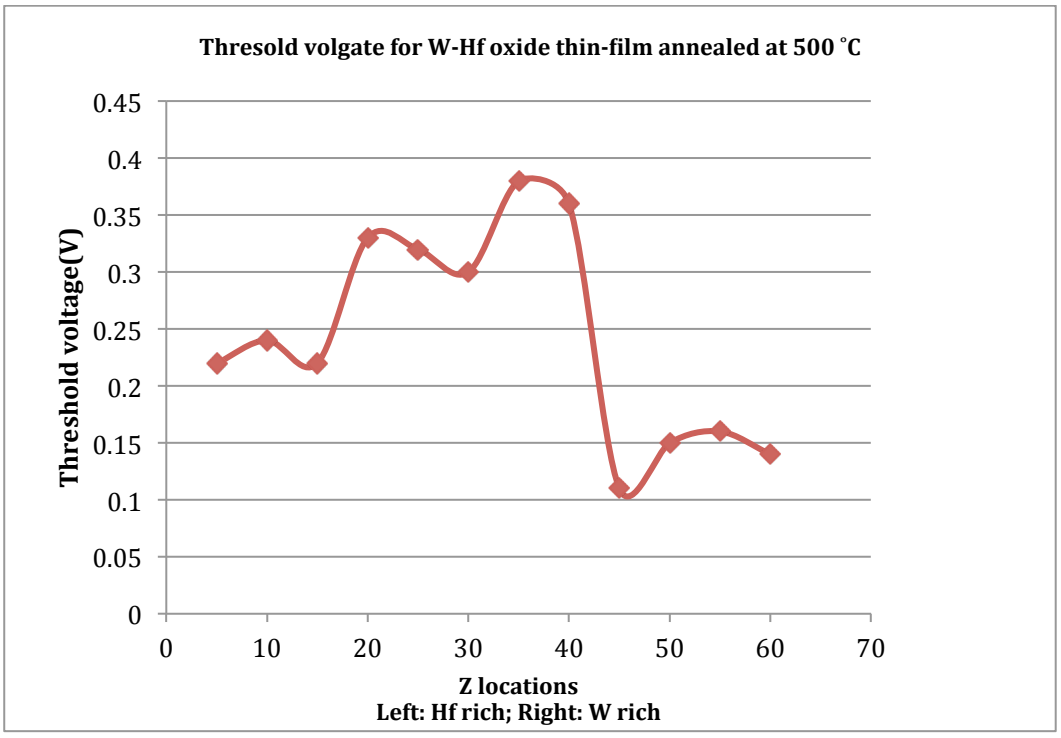

Figure 30 Photocurrents and threshold voltage for the W-Hf-O system are significantly degraded compared to undoped WO_3.

Related systems

Ta and Zr might be considered plausible alternatives to Hf for incorporation into WO_3, since they are close neighbors of Hf in the Periodic Table. However, films processed under conditions identical to those used for W-Hf-O were found to exhibit similarly poor stability upon annealing. One relatively intact W-Zr-O sample annealed at 500 ˚C was tested but was not found to exhibit any photoresponse. That is, no photocurrent was observed at any potential when irradiated by either the 405 nm or 532 nm lasers.

W-Fe-O and W-Cu-O

We explored the effect of adding Fe and Cu to WO_3, since both Fe_2O_3 and CuO have a band gap that is smaller than that of WO_3, and both have themselves been investigated as potential materials that would support photocatalytic activity over a relatively large region of the solar spectrum. We speculated that incorporation of Fe or Cu into the W-O system may lead to a $W_{1-x}Fe_xO_y$ or $W_{1-x}Cu_xO_y$ solid solution with a smaller band gap compared to undoped WO_3. CuO is known to exhibit poor stability in an in aqueous environment; it is unclear whether a $W_{1-x}Cu_xO_y$ solid solution could exhibit improved stability.

Stability

For preliminarily studies, W-Fe-O and W-Cu-O samples were annealed at 500 ˚C for 3 hours. Both films showed a good stability after annealing and electrochemical characterization. (Figure 31)

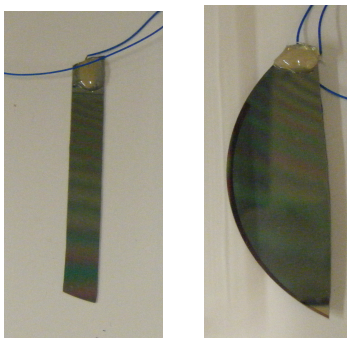

Figure 31 Left: W-Fe oxide thin film. Right: W-Cu oxide thin film. Both photos are of films after annealing at 500 ˚C followed by electrochemical characterization.

Photocatalytic properties

Under 405 nm illumination only a very small photocurrent was observed at any composition on either of the samples (Figure 32 and 33). Neither sample showed any photoactivity under illumination with the 532 nm laser, suggesting that the bandgap was no lower than 2.3 eV. Even at +0.5 V, they show very small photocurrent. Figure 32 shows the photocurrent measured at +0.5 V for the W-Cu-O sample slice annealed at 500 ˚C. The current observed for the most W-rich composition is much lower than for undoped WO_3, suggesting that Cu has a deleterious effect on photoactivity, perhaps by introducing recombination centers. However, the photocurrent at +0.5 V increases unmistakably as the Cu concentration increases, with a concomitant decrease in the threshold voltage. This suggests that Cu may be moving the band edge to a more favorable position. Further study is certainly indicated, including addressing the question of whether Cu incorporation leads to a change in crystal structure. In any case, the maximum photocurrent at +0.5 V, for any composition, is only 0.06 mA, which is much smaller than photocurrent measured for the WO_3 sample slice annealed at 500 ˚C.

Figure 33 shows the photocurrent measured at +0.5 V for the W-Fe-O sample. In this case we see that above a certain composition (corresponding to the position Z=40 mm) increasing the Fe concentration unambiguously degrades the activity of W-Fe-O. There appears to be an optimum Fe composition but this optimum is no better than undoped WO_3. This system could use further study.

The data for W-Cu-O and W-Fe-O suggest the possibility that improvements over the activity of WO_3 might be possible in these systems. Further study is indicated. It might be very enlightening to study films with higher crystallinity than these films annealed at only 500 ˚C, if films can be created that survive higher temperatures without delamination.

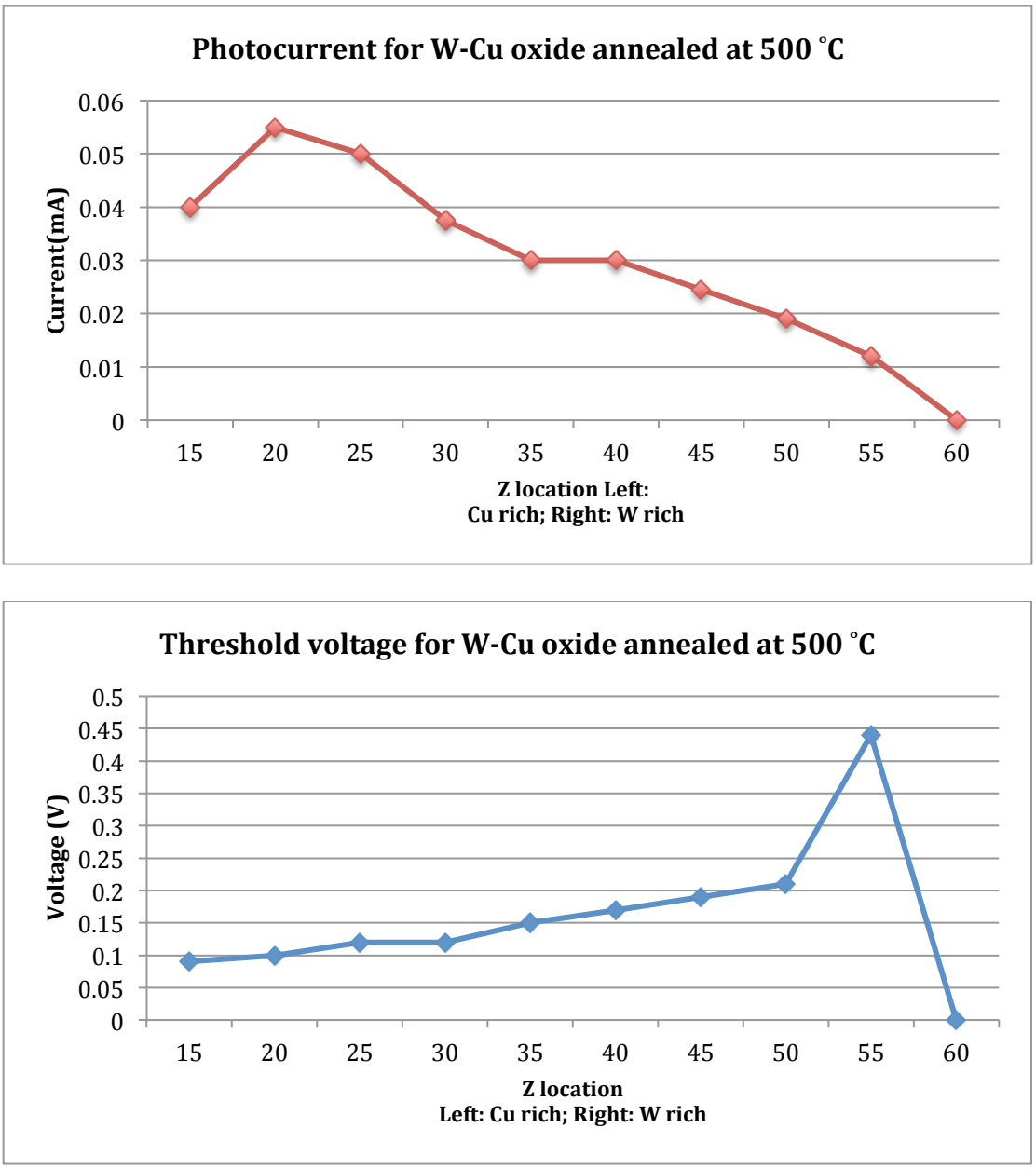

Figure 32 Photocurrents and threshold voltages for W-Cu-O annealed at 500 ˚C sample

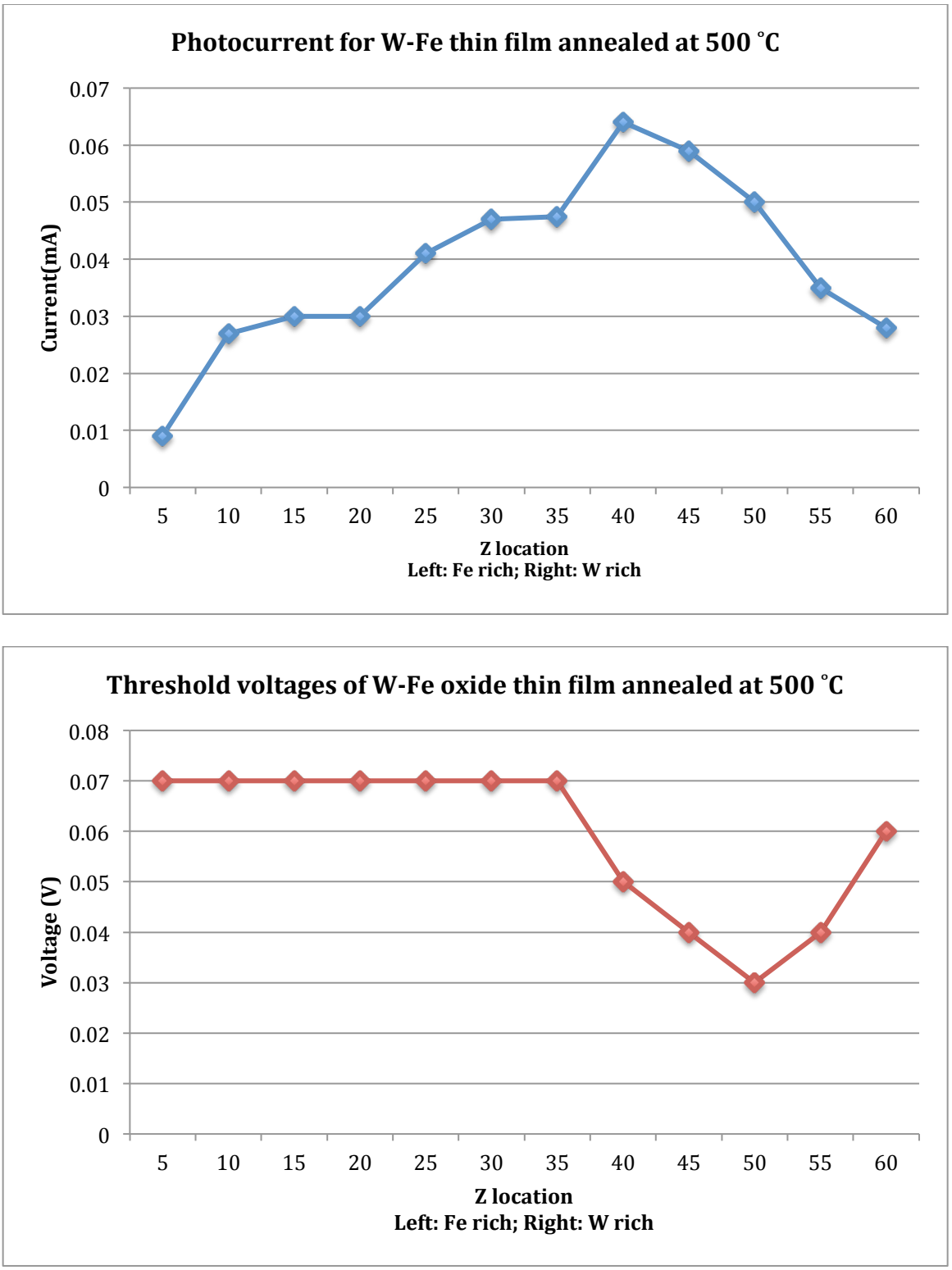

Figure 33 Photocurrents and threshold voltages for W-Fe-O annealed at 500 ˚C

W-Zn-O

Both tungsten oxide and zinc oxide are known photocatalytic materials that are effective under illumination by UV light. Coupled-semiconductor photocatalysts have been reported to have high performance for water purification. [15] With thise in mind, we studied the photoresponse performance of W-Zn-O binary thin films in neutral KDP buffer solution with 405 nm and 532 nm laser radiation.

Stability

The W-Zn-O system appears to be very stable for both annealing process and the electrochemical characterization, since no peeling or surface discoloration was observed. (Figure 34) This satisfies the first requirement to be a viable photocatalyst candidate, that must be durable in an aqueous environment.

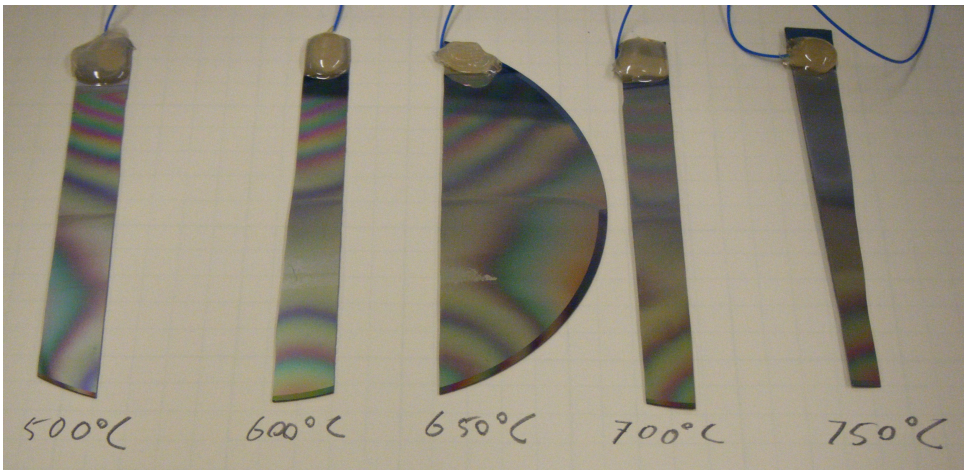

Figure 34 W-Zn-O samples after characterizations in pH=7 KDP buffer solution

Photocatalytic behavior—overview and comparison with other systems

W-Zn oxide thin film exhibited a photocatalytic behavior that is unique among all the samples we have tried in the research so far. Though no photocurrent was observed when illuminated by the 532 nm laser, W-Zn-O is the only system that shows photocurrent under 405nm radiation *at zero potential*. (Figure 35)

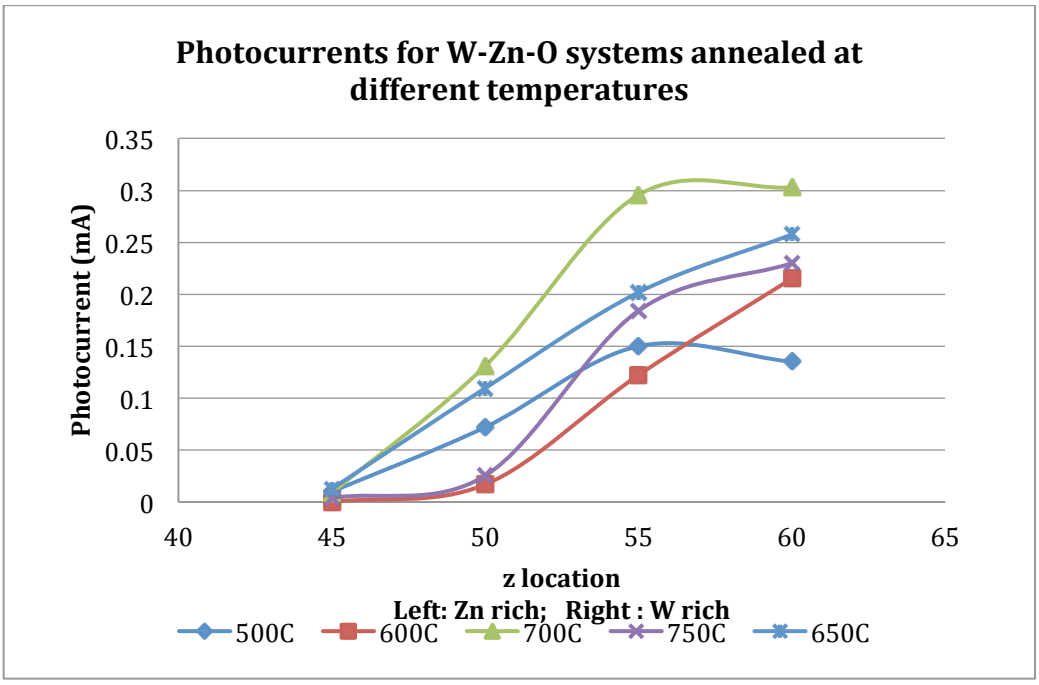

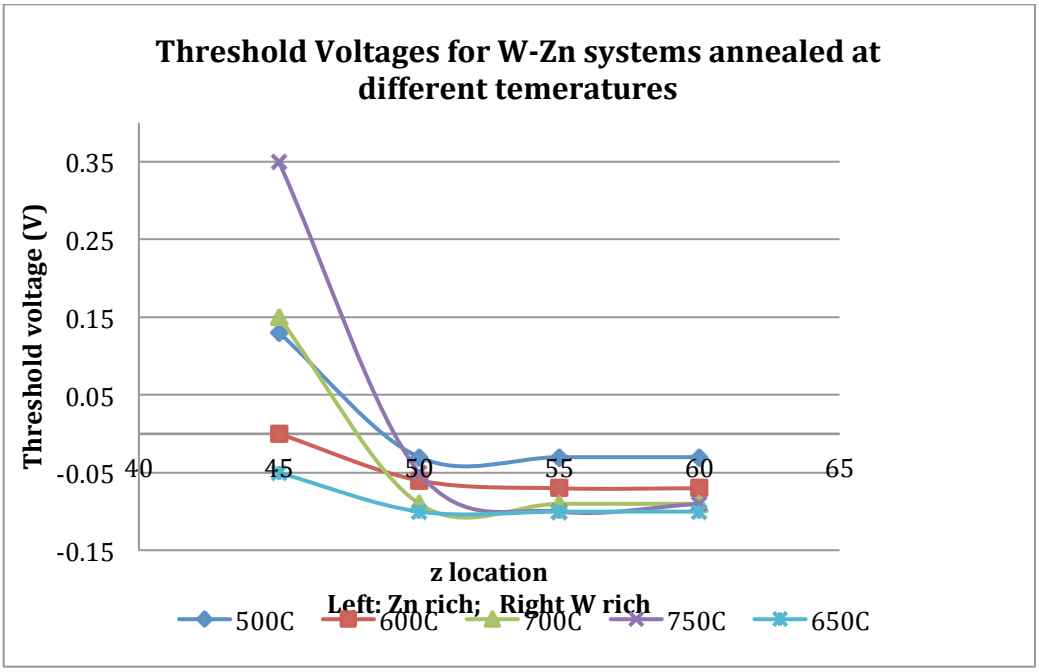

Figure 35 Photocurrents and threshold voltages for W-Zn samples annealed at different temperatures observed from characterization in pH=7 KDP buffer solution

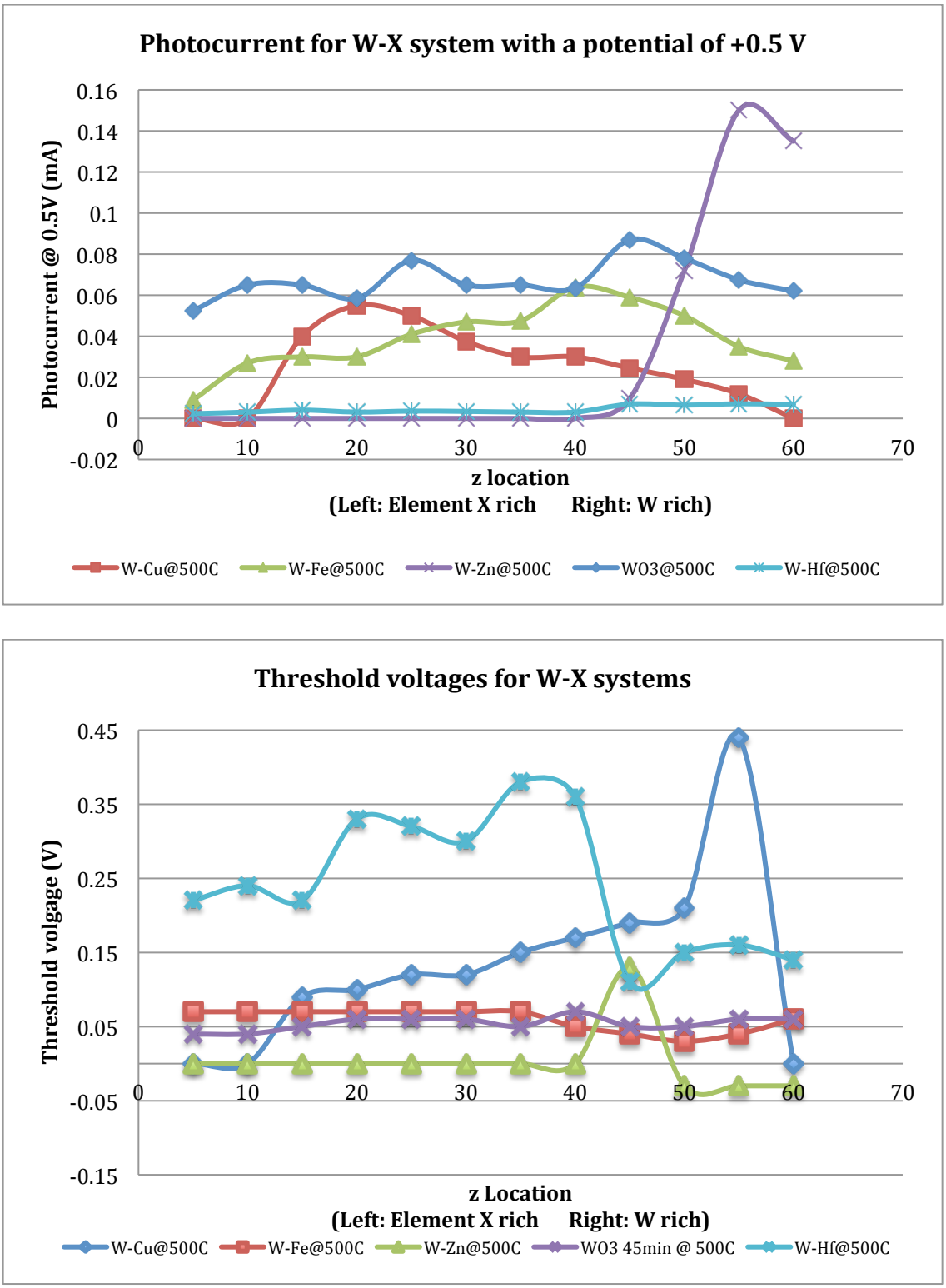

Figure 36 Photocurrents and threshold voltages for W-X systems annealed at 500 ˚C

(*W-Zn does not have data points for Z > 45)

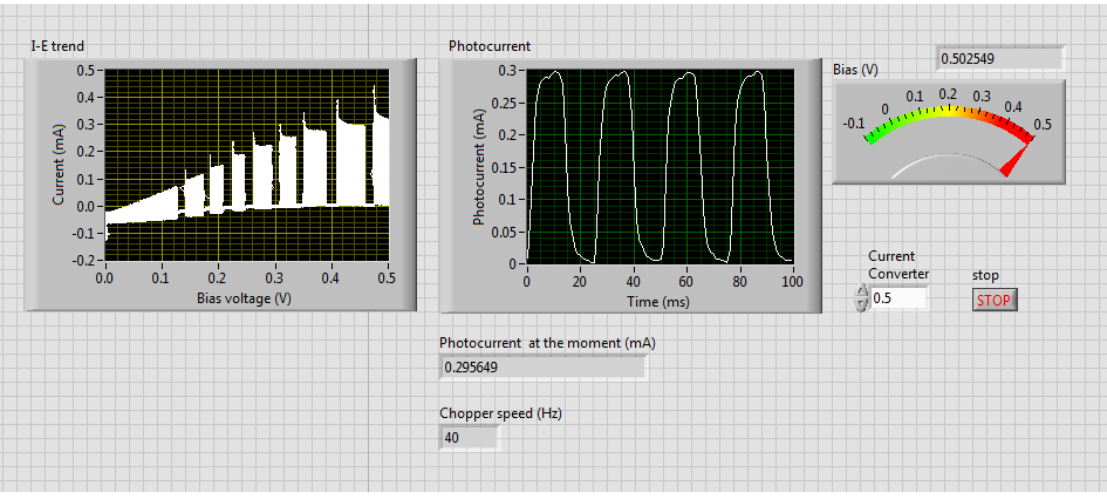

Figure 37 Photocurrent for W-Zn-O annealed at 700 ˚C. This screenshot shows data taken at position Z=60. The left hand plot show the current measured as a function of potential (upper envelope: laser on; lower envelope, dark; the laser is manually turned off for a few seconds at 8 points during the scan). The right-hand plot shows the time dependence of the photocurrent at about +0.5V as the laser is periodically interrupted by the SRS chopper.

W-rich compositions in the W-Zn-O system showed photocurrents much higher than undoped WO_3. (Figure 37) This may be due to changes in band location with respect to the reduction potential for O_2/H_2O redox couple, or it may indicating ta decrease in the overpotential for water oxidation. In any case the W-Zn-O system exhibits photocurrents at +0.5 V that are dramatically higher than those of any other system investigated, as shown in Figure 38.

Further discussion for W-Zn-O

In the initial study, the annealing temperature for the W-Zn-O thin film that gave the highest photocurrent was found to be 700 ˚C (Figure 35), and the composition with the maximum photocurrent in the film annealed at that temperature was found a the position Z=55, i.e., in the region that has a high W concentration. Since this region is close to the top edge of the film (Z=65), we decided to prepare a second composition spread that would be biased toward the W-rich region of composition space. This would allow us to examine W-rich

compositions in more detail and would provide confidence that composition is the variable that dominates the photocurrent behavior. To this end a second W-Zn-O samples was deposited using 100 W RF power applied to the W target and only 50 W RF power applied to the Zn target. All other parameters remained the same as the previous deposition. The second sample was annealed at 700 ˚C for 3 hours with a heating and cooling rate of 100 ˚C/h.

The behavior of the second sample is shown in Figure 38. The highest photocurrent at 0.5 V of the second sample was lower by a factor of 2 compared to the original sample. However the maximum photocurrent was observed at Z=30 —displaced to lower Z as expected since the Zn deposition rate was much lower. The lower value for maximum photocurrent might be attributed to the smaller thickness of the second film, which is to be expected because the Zn deposition rate was decreased.

Other factors that might affect the change in the photocurrent include a difference in defects and film morphology, including grain size and structure.

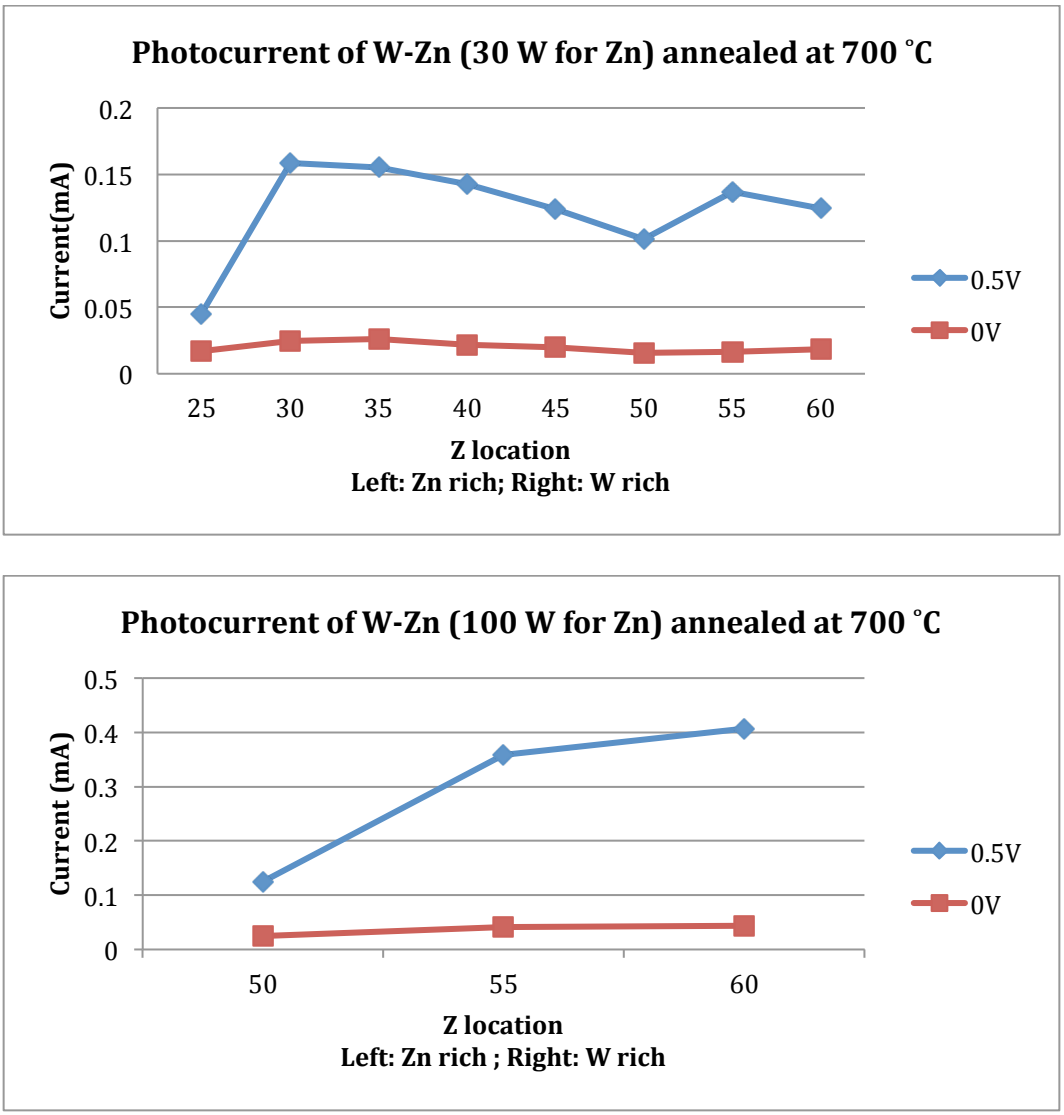

Figure 38 Photocurrent measured at 0.5 V and 0 V from the old and new samples

It is interesting that arc shaped fringes appear on all of our W-Zn-O samples after annealing process, apparently depending on composition and not on sputtering power nor annealing temperature. (Figure 39) The position of the fringe is approximately at the same position where photocatalytic response of the material changed dramatically. No photoactivity was exhibited at positions on the Zn-rich side of the arc, while on the W-rich side the activity increases with W concentration.

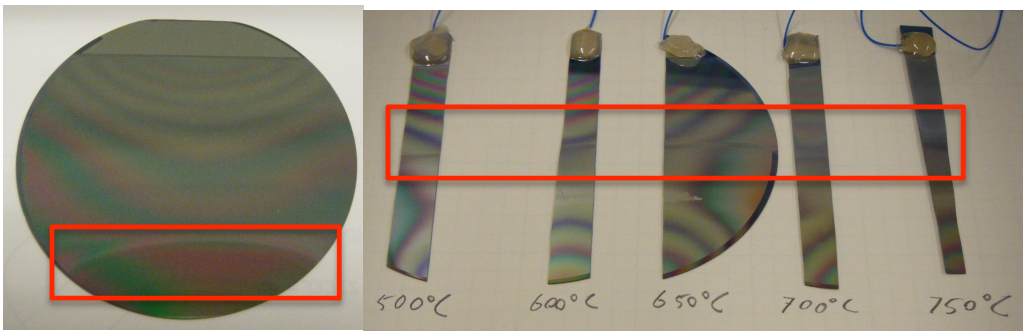

Figure 39 Left: Arc fringe on the W-Zn-O deposited with 100 W power for W, and 50 W power for Zn, and annealed at 700 ˚C. Right: Fringes on the sample slices annealed at different temperatures from the W-Zn-O sample deposited with 100 W power for both W and Zn.

3.2 Discussion on the experiment data

According to the well-established band structure of WO_3, its conduction band is located about 0.2 eV below the H^+/H_2O redox couple of water, as shown in Figure 5 and illustrated in Figure 40. To achieve H reduction using pure WO_3, a voltage more negative than about 0.2 V should be imposed onto the working electrode, assuming the band mismatch is the dominant factor preventing the reaction from happening. None of our WO_3 and W-X-O samples showed any photocurrent for negative potentials as great as -0.5 V vs. Ag/AgCl. However, our experimental is conducted at pH=7 rather than pH=0, so the equilibrium potentials must be adjusted using the Nernst equation. This means that the potential needed to achieve H reduction should be ~ -0.76 V vs SHE or ~ -0.96 V vs. Ag/AgCl. Therefore it is not surprising that no photocurrent is seen at -0.5 V.

On the other hand, the valence band of WO_3 is located well below the potential of the O_2/H_2O couple. During the photocatalytic process at neutral or positive potentials on the working electrode, holes in the material diffuse to the semiconductor/electrolyte interface to oxidize water to O_2, while electrons as

major charge carriers move through the circuit to the counter electrode to reduce H^+ ions to H_2, or to reduce O_2 dissolved in the buffer solution to O^{2-}. The water oxidation reaction is expected to be slow so overpotentials could be more significant here in our scenario, and might be the factor responsible for the observation that in many cases a robust positive potential is required to see a measurable photocurrent. Indeed, data reported in the literature are consistent with this observation. Figure 40 reproduces typical data showing an onset of photocurrent for WO_3 at V= +0.3 V. (The current seen for negative potentials is independent of illumination; it is not due to H oxidation but is instead attributed to formation of a hydrogen tungsten bronze.) Hydrogen generation at the counter electrode has been reported, confirming the interpretation of the origin of photocurrent. (Figure 41)

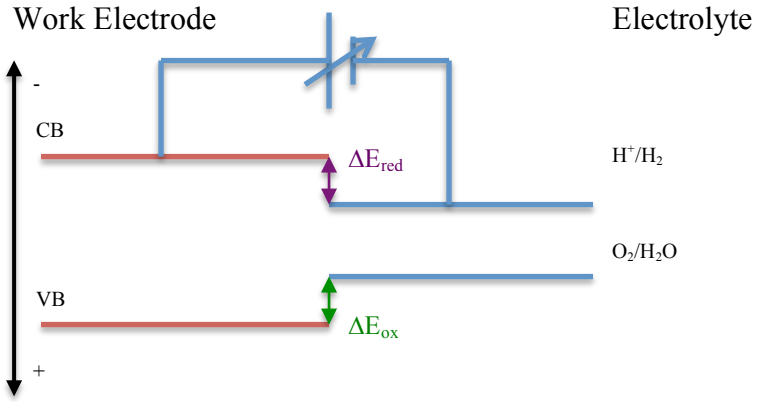

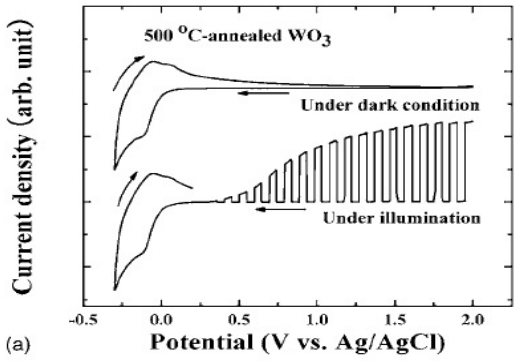

Figure 40 Photo-response of a 500 ˚C- annealed WO_3 film in wide potential range of -0.3 V to +2 V under dark condition and light on/ off illumination, as reported in Ref. [16]

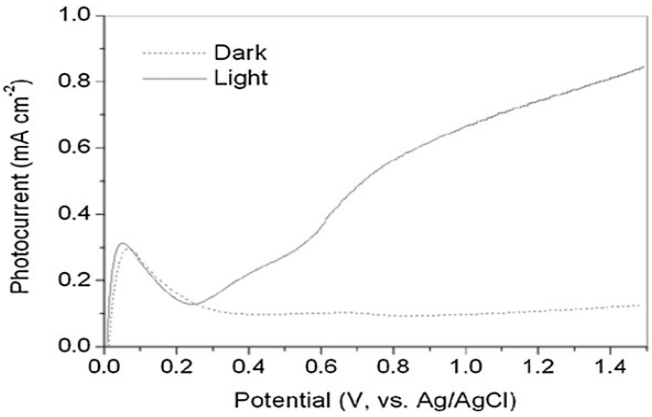

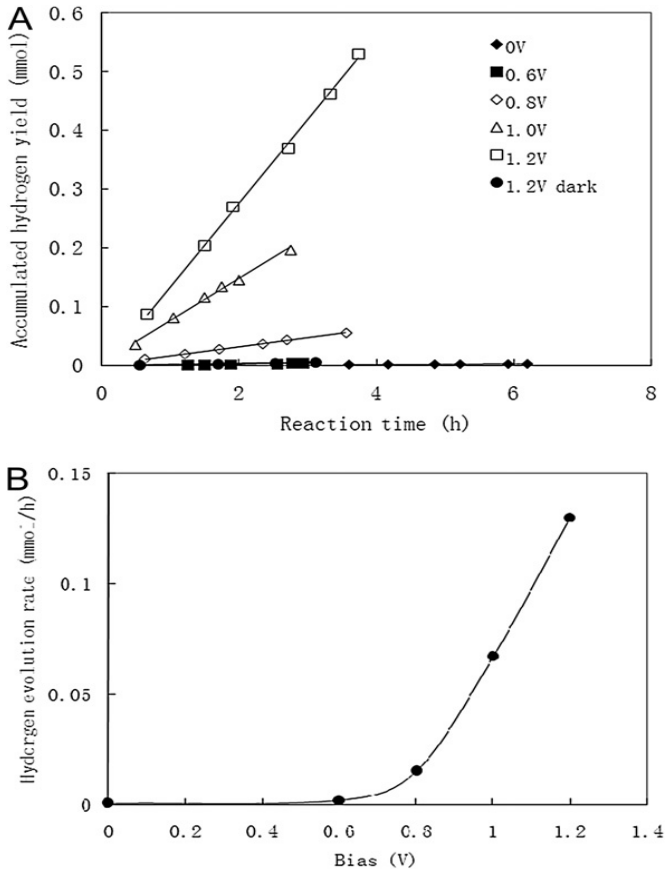

Figure 41 Up: Current- Voltage characteristics of tungsten oxide film in 0.5 M H_2SO_4 aqueous solution under dark and 0.1 Wcm^{-2} Xe light irradiation. The scan rate was 5 mV/s. Down: Hydrogen evolution test at different applied voltages using Xe lamp as a light source.[17]

The Appendix details some of the experiments used to confirm the basic nature of the results reported here, since the experimental setup was newly constructed, and needed to be verified to be operating correctly. Experiments were done on working electrodes including Pt, WO_3 annealed at 700 ˚C and W-Zn-O annealed at 700 ˚C. We did cyclical voltammetry under continuous light-on and light-off conditions as well as CV measurements with chopped light on/off irradiation. The results are completely consistent with the literature.[18], [19], [20], [21], [22], [23].

In any case the central result of this work, namely that Zn-substituted WO_3 films exhibit much higher photoactivity than undoped WO_3, cannot be questioned. The threshold for activity occurs at a lower potential, and at high potentials the photocurrent is much higher in the Zn-substituted WO_3 films. Preliminary X-ray diffraction studies suggest that the best material exhibits the WO_3 structure, though good activity is observed even for structures more related to $ZnWO_4$.

4. Conclusions

Band gap engineering techniques for development of oxide semiconductor thin-film for photocatalyst has been reviewed. A photoelectrochemical characterization system enabling automated measurement of CV curves and photocurrent on thin-film combinatorial libraries deposited on pre-treated silicon wafers has been established. A number of binary tungsten oxide thin-film samples have been processed and measured, and among these we discovered a W-oxide-based material with photoactivity for water oxidation at a record low potential for a W-O-based material: W-Zn-O. The best annealing temperature for this binary system was determined to be 700 ˚C. Preliminary crystallographic studies are inconclusive but suggest that the highest performance is obtained for Zn-substituted WO_3.

5. Future directions

The work reported here represents the beginning of the ability to systematically characterize photoactivity in novel materials, and initial identification of the W-Zn-O system as a promising material for photocatalysis. a more detailed understanding of the composition dependence of photoactivity is clearly warranted. In particular, it is important to generate a robust understanding of the crystal structure that is obtained as a function of composition, so that structure/property relations can be described. One clue might come from an understanding of the significance of the arc-shaped fringe seen in Zn-rich compositions. Further band gap engineering and surface modification steps sould be taken in the future research based on W-Zn-O system to develop photocatalysts for solar hydrogen production. Incorporating p-block nonmetals such as N could raise the valence band potential and reducing the band gap.

In terms of the experimental apparatus, it would be useful to implement fully automated measurement following a scripted set of X and Z positions and potential. This level of automation would enable scanning of the ternary combinatorial samples. The improvement in the characterization system would also include new LabVIEW VIs that present the distribution of photocurrent at a chosen voltage using an intensity graph. This would help us better visualize and understand the influence of on hickness and composition on photocatalytic activity. We should also develop a method to measure the power of photon beams incident on the wafer (in the electrolyte) so that a reasonably accurate

efficiency calculation can be made UV-Vis spectroscopy as a function of position would be useful for determining the band gap of the oxide as well as the absorption length, which would aid in interpreting photocatalytic results.

6. Appendix

In this chapter, we present detailed data from our experiments aiming at confirming basic observations in our study, comparing them with those reported from other literatures, and reconciling the discrepancy between experimental photocurrent and predicted band alignment.

Pt

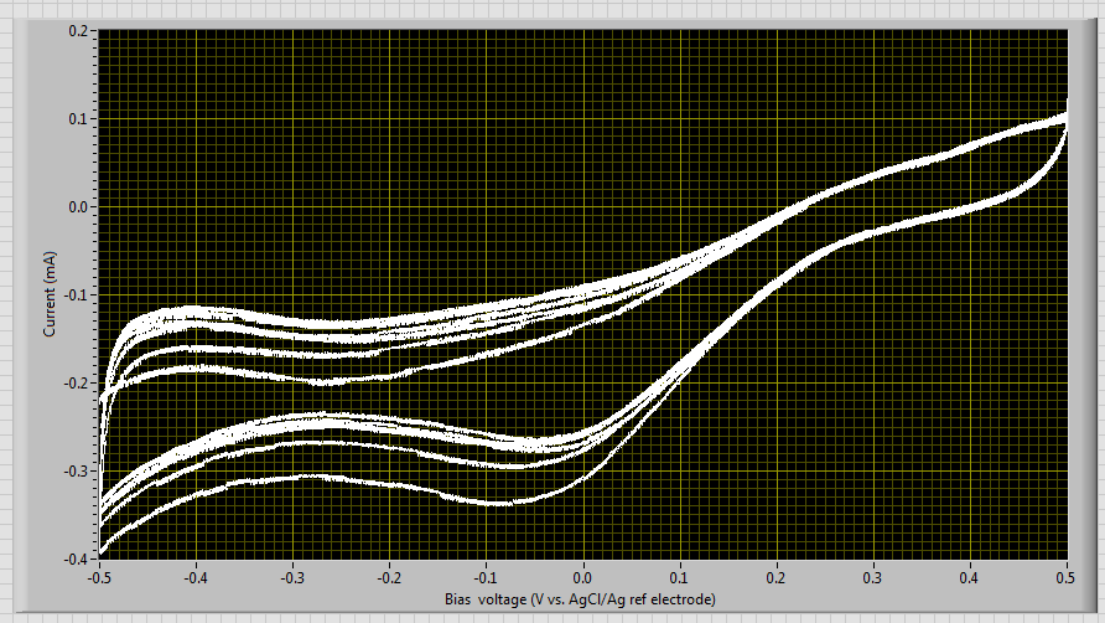

Figure 42 CV curve for Pt working electrode between -0.5 V and +0.5 V, voltage ramping at 250 mV/s. No obvious difference is observed during the process when the laser was turned on or off.

Cyclic voltammetry is done with a ramping speed of 250 mV/s for Pt working electrode in pH=7 KDP buffered solution between – 0.5 V and + 0.5 V. Totally 6 cycles of ramping were done. Not illumination was made to the Pt electrode for the first 3 ramps, while 405 nm laser radiation was light on the working electrode. From the graph, we find no obvious change cause from the 405 nm illuminations. The positive potential area of the CV curves overlapped together, while the negative part shows very small difference, because of the

capacitance of the electrolyte at fast voltage ramping. This CV curve is used as a control to in the whole verification experiments to further legitimate our observations reported earlier. (Figure 42)

WO3 annealed at 700 ˚C

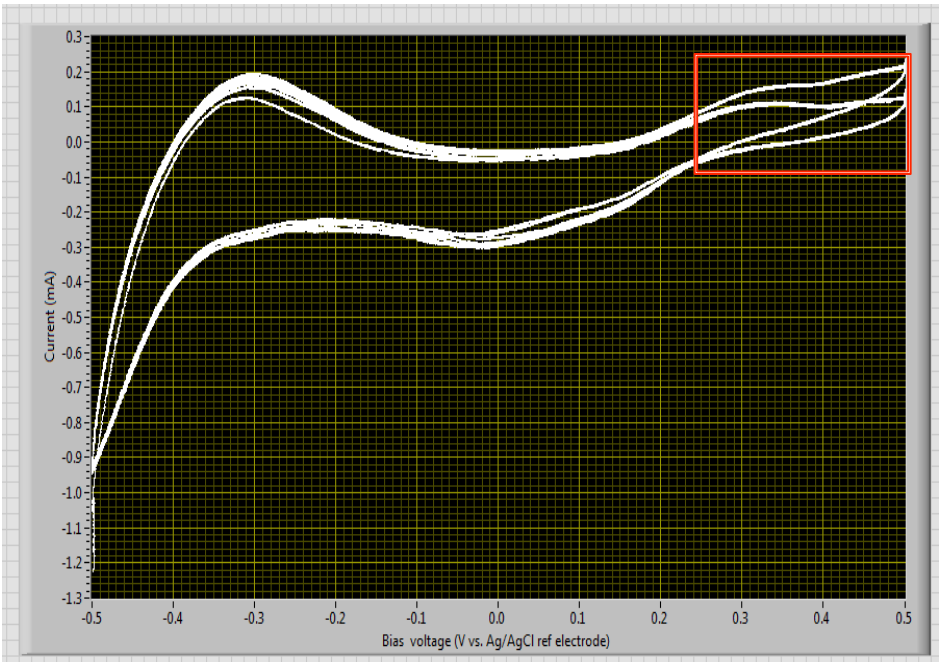

Figure 43 CV for tungsten trioxide thin- film annealed at 700 ˚C. Voltage ramped at 100 mV/s. The consequence on current from light on and off is easy to see in the area within the red square.

CV measurement is done between – 0.5 V and 0.5 V with a speed of 100 mV/s on z = 50 for WO_3 annealed at 700 ˚C sample. To reduce the effect from capacitance because of a too high voltage ramping, a slower ramping rate is applied here. Like the Pt control measurement, in the total 6 ramps, the first 3 scans were done without illumination, while the last 3 were under the 405 nm laser radiation. Intensified current signal as a result of the illumination has been observed at positive potentials. The whole CV pattern of the illuminated ramps is moves upward, and this effect can be clearly observed from Figure 43. An enlarged plot for the area in the square of Figure 43 is presented in Figure 44, so

details of the effect from illumination in CV measurement for tungsten oxide can be observed easily. Light on / off signals can also be observed as we switch on and off the laser during an identical CV experiment. (Figure 45) Conventional light on/ off signal in a single direction potential ramping is also studied in our experiments and their results for tungsten oxide sample are shown in Figure 46 and Figure 47.

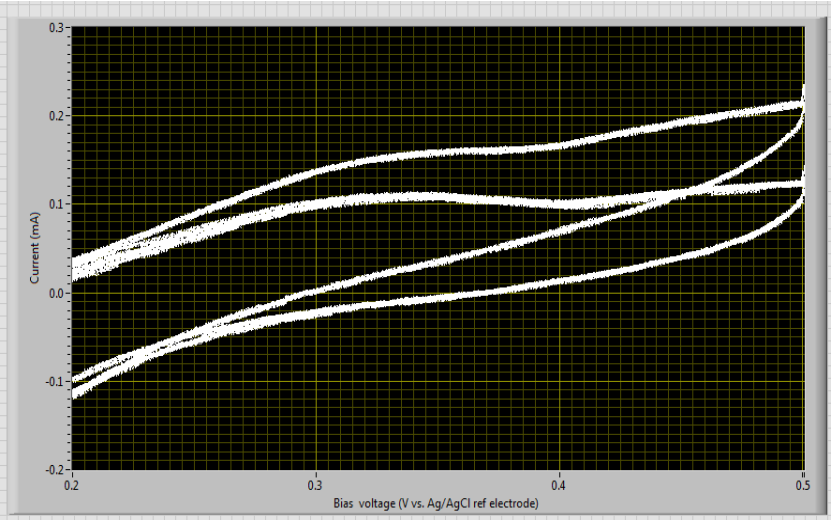

Figure 44 Enlarged image of the area in the red square.

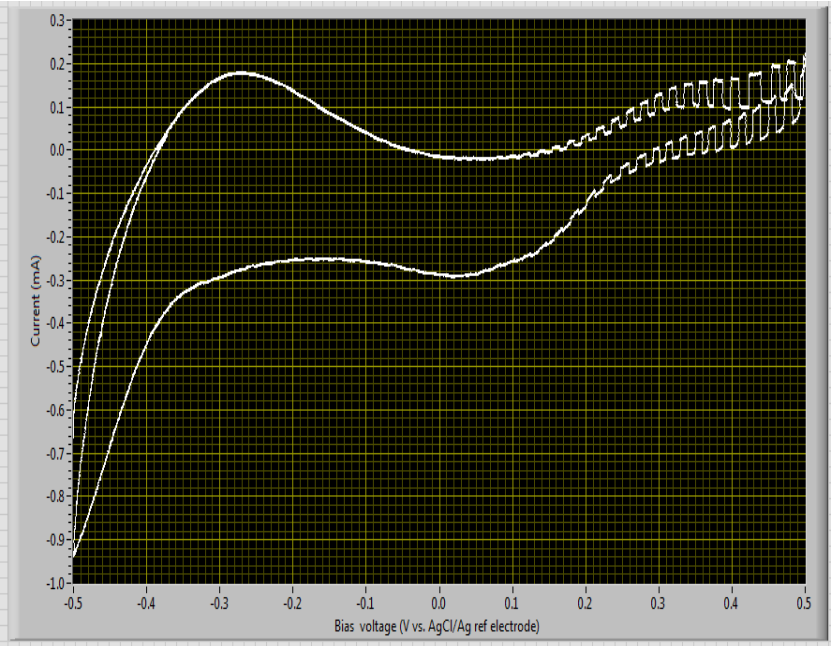

Figure 45 Light on/ off CV for WO_3 annealed at 700 ˚C. Voltage ramping at 100 mV/s

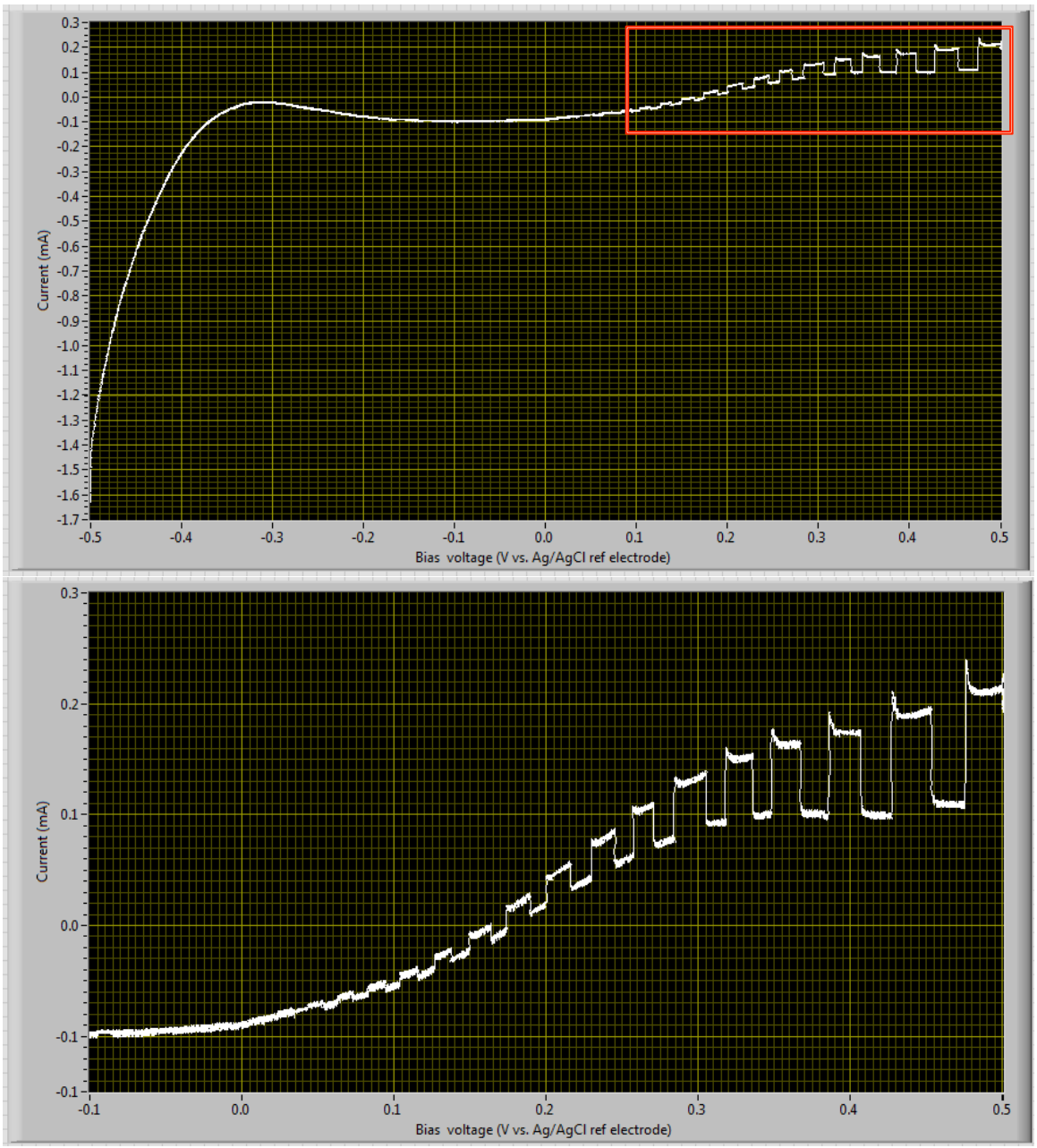

Figure 46 Up: Light on and off signal for WO_3 annealed at 700 ˚C when voltage ramping from -0.5 V to 0.5 V. Down: Enlarged image for area in the red square.

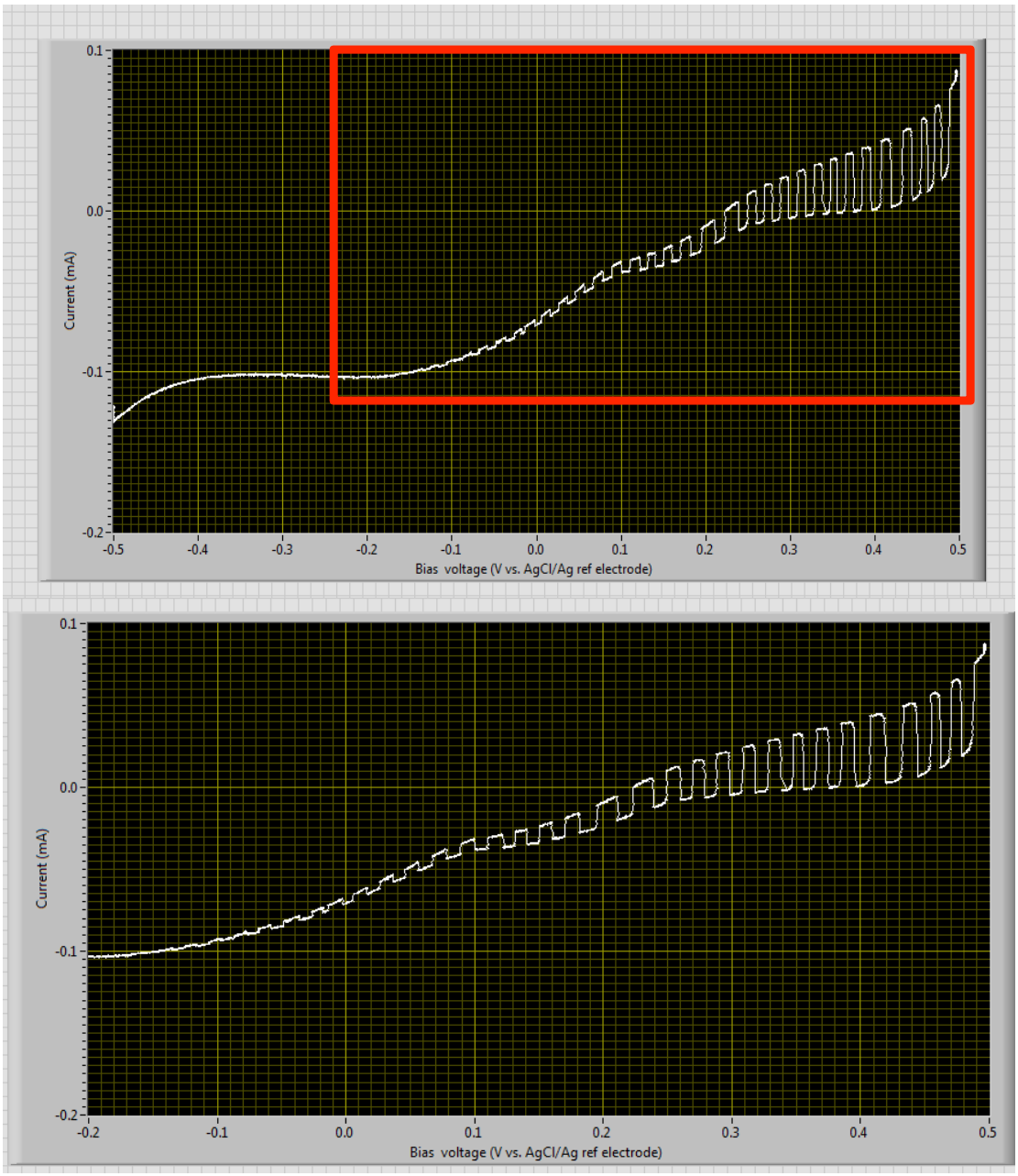

Figure 47 Up: Photocurrent signals for WO_3 annealed 700 ˚C, when the voltage was ramping down from +0.5 V to -0.5 V at a speed of 100 mV/s. Down: Enlarged area in the red square, which reveals that the photocurrent starts to show up at around -0.06 V, and enhanced when potential goes positively.

W-Zn-O thin film annealed at 700˚C

CV and single direction voltage ramping with exactly the same condition as the previous WO_3 sample are done to the W-Zn-O annealed at 700 ˚C sample. 405 nm laser was shined on z = 55 point on the sample. Impressive effect caused by illumination during a CV measurement can be seen in Figure 48, where the exposure to laser not only intensified the current at positive potential but also result in a significant change for the negative potential area. This is amazing, since it bolstered our previous claim that this binary oxide photocatalytic system have a negative onset potential, and can significantly enhance the photo-response. The effect of illumination by the 405 nm laser is further presented vividly in Figure 49, where conventional light on/ off signal is modulated, by switching on and off the laser periodically during the potential ramping. It clearly shows that the threshold potential for this oxide system is at a negative location. Single direction voltage ramps are also done to reveal the precise value for this onset potential. These results are presented in Figure 50, 51 and Figure 52. From Figure 52 we can confirm that the onset potential for z = 55 on W-Zn-O annealed at 700 ˚C is – 0.13 V.

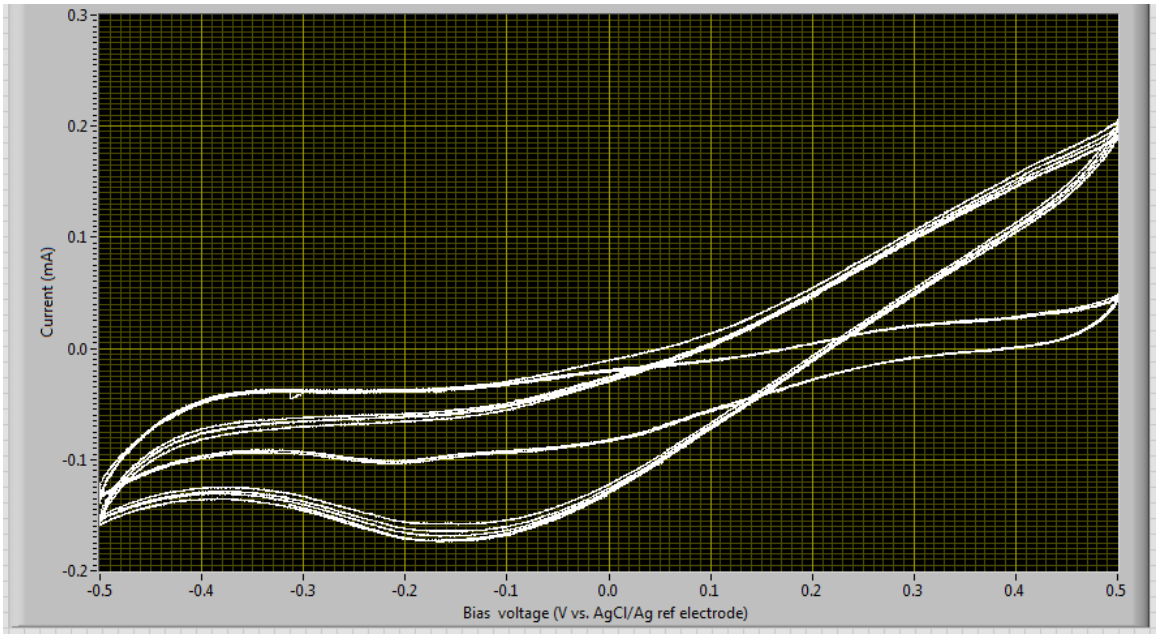

Figure 48 CV for W-Zn-O (W: 100 W, Zn: 100 W) annealed at 700 ˚C, voltage ramping at 100 mV/s. Light on and off can be easily distinguished. (Upper one is the curve when light is on)

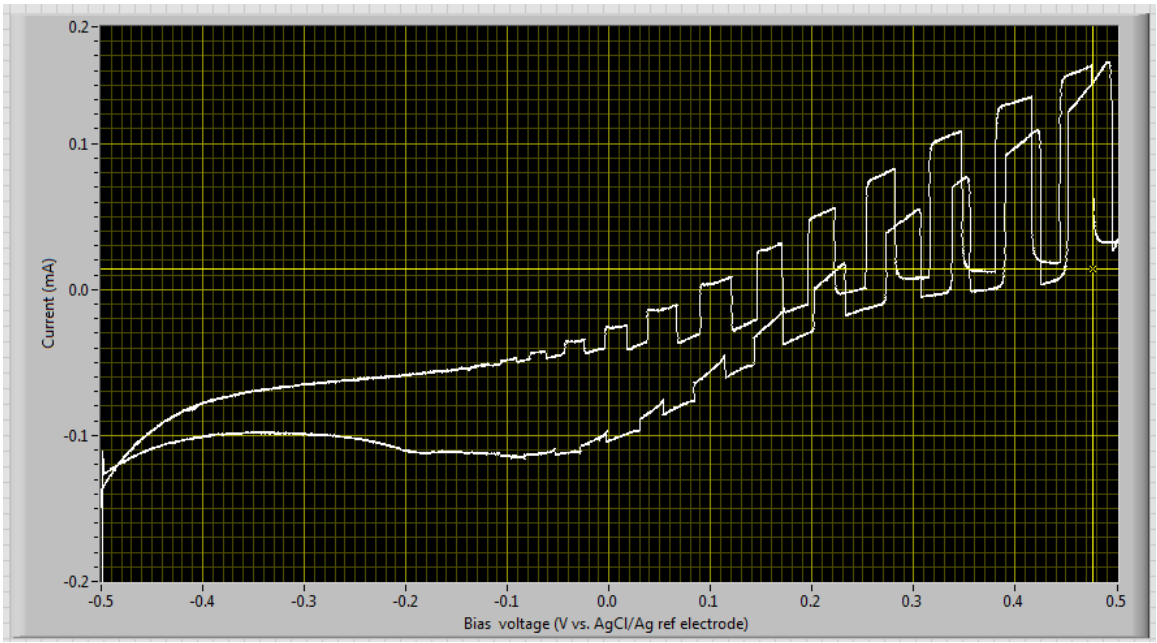

Figure 49 CV for W-Zn-O (W: 100 W, Zn: 100 W) annealed at 700 ˚C. Beam switched on and off periodically during the whole process. Voltage ramped at 100 mV/s.

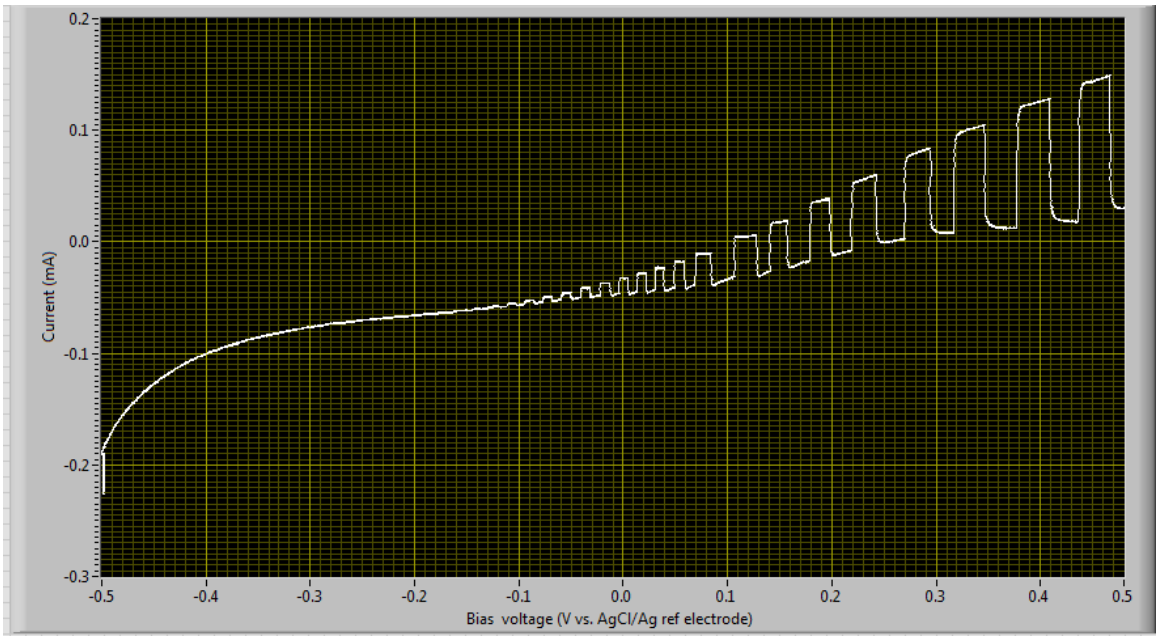

Figure 50 Photocurrent signals for W-Zn-O annealed at 700 ˚C sample when ramping voltage up at 100 mV/s

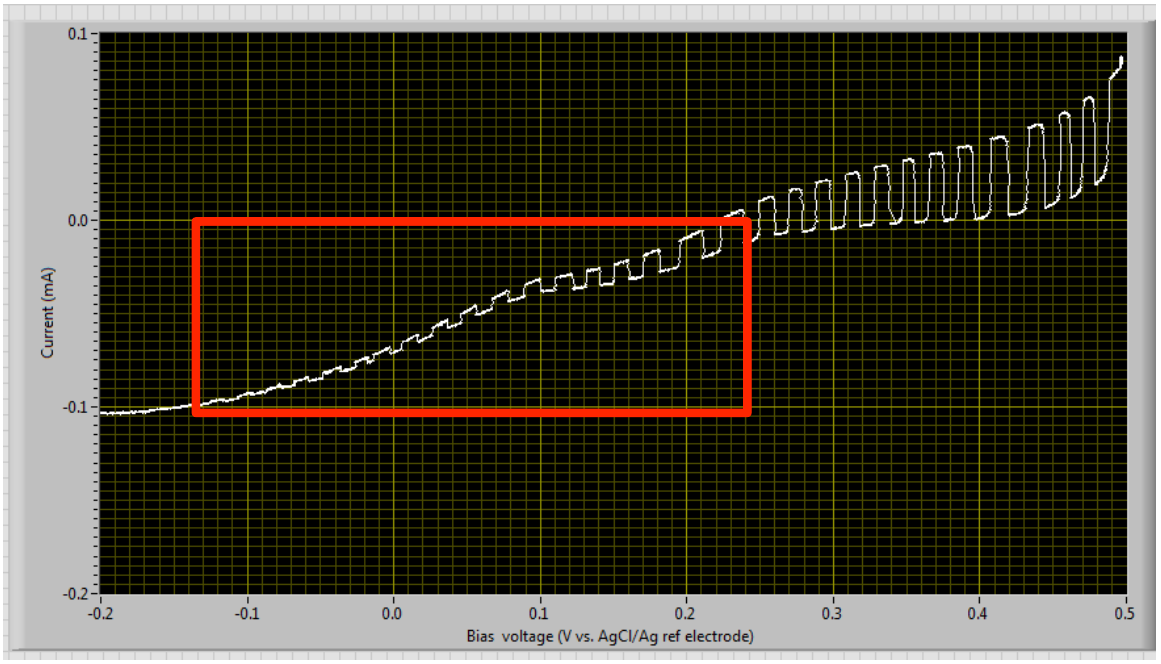

Figure 51 Photocurrent signals for W-Zn-O annealed at 700 ˚C sample when ramping voltage down at 100 mV/s

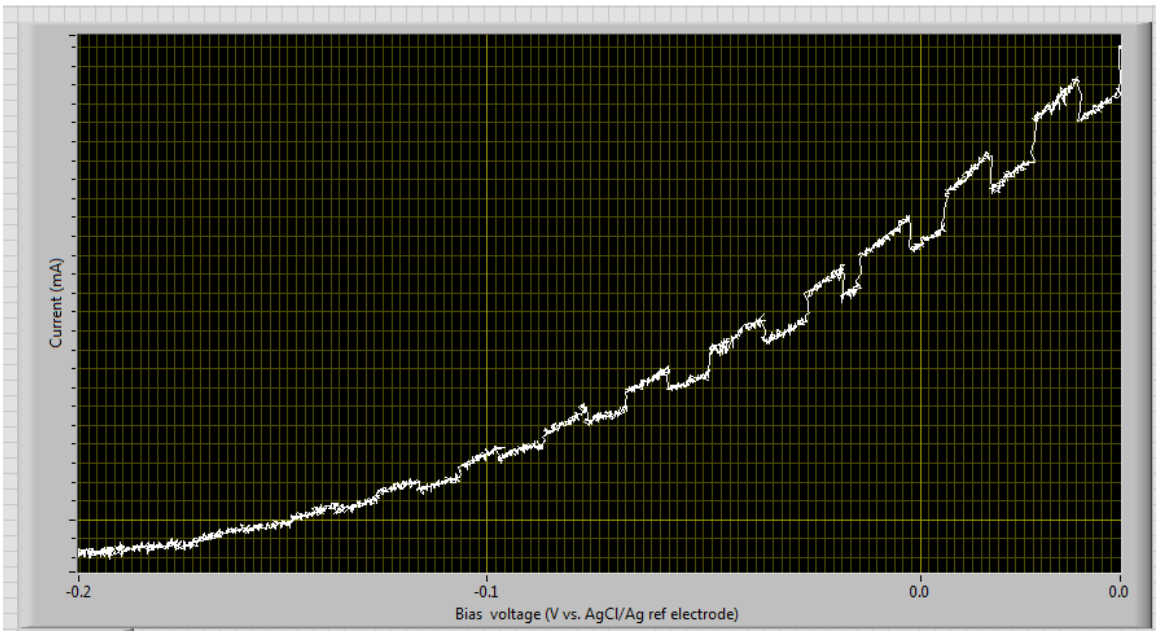

Figure 52 Enlarged area in the red square fro Figure 53 showing the cutting off voltage (also the threshold voltage) is at around -0.13 V

Our verification experiments showed the consistency of our data presented in the thesis. Also it showed uniqueness of W-Zn-O binary oxide system in photocatalytic property.

7. Reference

[1] J. Wiley, *Principles and applications of photochemistry*. London, 2009.

[2] K. Fujishima, Akira; Honda, "Electrochemical Photolysis of Water at a Semiconductor Electrode," *Nature*, vol. 238, 1972.

[3] K. Maeda and K. Domen, "Photocatalytic Water Splitting: Recent Progress and Future Challenges," *The Journal of Physical Chemistry Letters*, vol. 1, no. 18, pp. 2655–2661, Sep. 2010.

[4] X. Chen, S. Shen, L. Guo, and S. S. Mao, "Semiconductor-based Photocatalytic Hydrogen Generation," pp. 6503–6570, 2010.

[5] K. Biernat and A. Malinowski, "The Possibility of Future Biofuels Production Using Waste Carbon Dioxide and Solar Energy," 2013.

[6] A. Paracchino, V. Laporte, K. Sivula, M. Grätzel, and E. Thimsen, "Highly active oxide photocathode for photoelectrochemical water reduction.," *Nature materials*, vol. 10, no. 6, pp. 456–61, Jun. 2011.

[7] A. Kudo and Y. Miseki, "Heterogeneous photocatalyst materials for water splitting.," *Chemical Society reviews*, vol. 38, no. 1, pp. 253–78, Jan. 2009.

[8] F. Wang, X. Chen, X. Hu, K. S. Wong, and J. C. Yu, "WO3/TiO2 microstructures for enhanced photocatalytic oxidation," *Separation and Purification Technology*, vol. 91, pp. 67–72, May 2012.

[9] R. M. Navarro, M. C. Alvarez-Galván, J. a. Villoria de la Mano, S. M. Al-Zahrani, and J. L. G. Fierro, "A framework for visible-light water splitting," *Energy & Environmental Science*, vol. 3, no. 12, p. 1865, 2010.

[10] Y. Inoue, "Photocatalytic water splitting by RuO2-loaded metal oxides and nitrides with d0- and d10 -related electronic configurations," *Energy & Environmental Science*, vol. 2, no. 4, p. 364, 2009.

[11] F. Wang, C. Di Valentin, and G. Pacchioni, "Doping of WO 3 for Photocatalytic Water Splitting : Hints from Density Functional Theory," 2012.

[12] J. Ouellette, "Combinatorial materials synthesis," *The industrial physicist*, vol. 9, no. 12, pp. 24–27, 1998.

[13] Q. (Sandia L. Butler, M.A., R. D. Rasby, Rod K, "(Received 31 March 1976; in revised form 3 May 1976 by A. A. Maradudin)," *Solid State Communications*, vol. 19, pp. 1011–1014, 1976.

[14] F. Wang, C. Di Valentin, and G. Pacchioni, "Rational Band Gap Engineering of WO3 Photocatalyst for Visible light Water Splitting," *ChemCatChem*, vol. 4, no. 4, pp. 476–478, Apr. 2012.

[15] C. Yu, K. Yang, Q. Shu, J. C. Yu, F. Cao, and X. Li, "Preparation of WO3/ZnO Composite Photocatalyst and Its Photocatalytic Performance," *Chinese Journal of Catalysis*, vol. 32, no. 3–4, pp. 555–565, Jan. 2011.

[16] K. Ahn, S. Lee, A. C. Dillon, C. E. Tracy, and R. Pitts, "The effect of thermal annealing on photoelectrochemical responses of WO 3 thin films," pp. 1–4, 2007.

[17] W. Zhao, Z. Wang, X. Shen, J. Li, C. Xu, and Z. Gan, "Hydrogen generation via photoelectrocatalytic water splitting using a tungsten trioxide catalyst under visible light irradiation," *International Journal of Hydrogen Energy*, vol. 37, no. 1, pp. 908–915, 2011.

[18] S. Berger, H. Tsuchiya, A. Ghicov, and P. Schmuki, "High photocurrent conversion efficiency in self-organized porous WO3," vol. 203119, pp. 88–91, 2006.

[19] H. Kim, K. Senthil, and K. Yong, "Photoelectrochemical and photocatalytic properties of tungsten oxide nanorods grown by thermal evaporation," *Materials Chemistry and Physics*, vol. 120, no. 2–3, pp. 452–455, 2010.

[20] M. R. Waller, T. K. Townsend, J. Zhao, E. M. Sabio, R. L. Chamousis, N. D. Browning, and F. E. Osterloh, "Oxidation in the Quantum Confinement Regime," 2012.

[21] N. Gaillard, Y. Chang, J. Kaneshiro, A. Deangelis, and E. L. Miller, "Status of Research on Tungsten Oxide-based Photoelectrochemical Devices at the University of Hawai ' i," vol. 7770, pp. 1–14, 2010.

[22] N. N. Metals and I. Company, "High Photocatalytic Capability of Self-Assembled Nanoporous WO 3 with Preferential Orientation of (002) Planes," no. 002.

[23] A. Tacca, L. Meda, G. Marra, A. Savoini, S. Caramori, V. Cristino, A. Bignozzi, G. Pedro, and P. P. Boix, "Photoanodes Based on Nanostructured WO 3 for Water Splitting," pp. 3025–3034, 2012.